P wave tomography of the mantle under the Alpine-Mediterranean area

Claudia Piromallo and Andrea Morelli
Istituto Nazionale di Geofisica e Vulcanologia, Rome, Italy

Received 10 January 2002; revised 5 June 2002; accepted 9 September 2002; published 1 February 2003.

[1] We study the upper mantle *P* wave velocity structure below the Euro-Mediterranean area, down to 1000 km depth, by seismic travel time tomography. We invert summary residuals constructed with both regional and teleseismic first arrival data reported by the International Seismological Centre (ISC) (1964–1995), introducing some alternative strategies in the travel time tomographic approach and a new scheme to correct teleseismic data for global mantle structure. Our high-resolution model PM0.5 is parameterized with three-dimensional (3-D) linear splines on a grid of nodes with 0.5° spacing in both horizontal directions and 50 km vertical spacing. We obtain about 26% root-mean-square (RMS) reduction of residuals by inversion in addition to roughly 31% reduction after summary rays formation and selection. Sensitivity analyses are performed through several test inversions to explore the resolution characteristics of the model at different spatial scales. The distribution of large-scale fast anomalies suggests that two different stages of a convection process presently coexist in very close regions. The mantle dynamics of western central Europe is dominated by blockage of subducted slabs at the 660 km discontinuity and ponding of seismically fast material in the transition zone. Contrarily, in the eastern Mediterranean, fast velocity material sinks into the lower mantle, suggesting that the flow of the cold downwelling here is not blocked by the 660 km discontinuity. On a smaller scale, the existence of tears in the subducted slab (lithospheric detachment) all along both margins of the Adriatic plate, as proposed by some authors, is not supported by our tomographic images. *INDEX TERMS:* 7203 Seismology: Body wave propagation; 7218 Seismology: Lithosphere and upper mantle; 8180 Tectonophysics: Evolution of the Earth: Tomography; 9335 Information Related to Geographic Region: Europe; *KEYWORDS:* travel time, body wave tomography, upper mantle, Europe-Mediterranean area, Earth structure

Citation: Piromallo, C., and A. Morelli, *P* wave tomography of the mantle under the Alpine-Mediterranean area, *J. Geophys. Res.*, *108*(B2), 2065, doi:10.1029/2002JB001757, 2003.

1. Introduction

[2] The Alpine-Mediterranean region developed under continuous rearrangement with time of the oceanic space during the progressive shortening of the Tethyan belt. The closure of the Tethys ocean started with subduction of oceanic lithosphere below the southern Eurasian plate at the time of opening of the central Atlantic (Jurassic–Cretaceous boundary, about 140 Myr), and continued until the beginning of Oligocene. On the site of this Mesozoic seaway, several stages of subduction, oceanic accretion and continental collision, originated the main tectonic features of a complex domain. A location map and names of the main tectonic units are given in Figure 1a. Large-scale reconstructions of the evolution of the Alpine-Mediterranean region, based on syntheses of kinematic, paleomagnetic, and geological data, are discussed by *Dercourt et al.* [1986] and *Dewey et al.* [1989] and, in spite of the many unsolved uncertainties, are widely accepted in their main points. Before Oligocene, though continental collision was already present between Apulia and Eurasia, and between Arabia and Eurasia, most of the convergence was taken up by sinking of oceanic lithosphere along the Eurasian active margin. The tectonic style east of Apulia was subduction dominated. During Oligocene, oceanic basins remained progressively trapped in a wide area, which later on, by Early Miocene, underwent the passage from subduction-dominated to continental collision-dominated convergence. The orogenic activity in the Alps and the Pyrenees was paralleled by the development of the European Cenozoic Rift System (ECRIS) [*Ziegler*, 1992]. The formation of the Apennines began through northwestward subduction of oceanic lithosphere and eastward migration of the trench. After Oligocene, to the east, subduction progressed below the Hellenic-Cyprean Arc and Taurides, possibly initiated in the Black and southern Caspian Seas, and ceased in the Dinarides and Pontides. To the west, by Early Miocene, extension between the Sardinia-Corse Block and Iberia determined the formation of new oceanic crust and opening of the Ligurian and Alboran Sea. The Tyrrhenian Sea opened during late Miocene to Pliocene, as a later exten-

0148-0227/03/2002JB001757$09.00

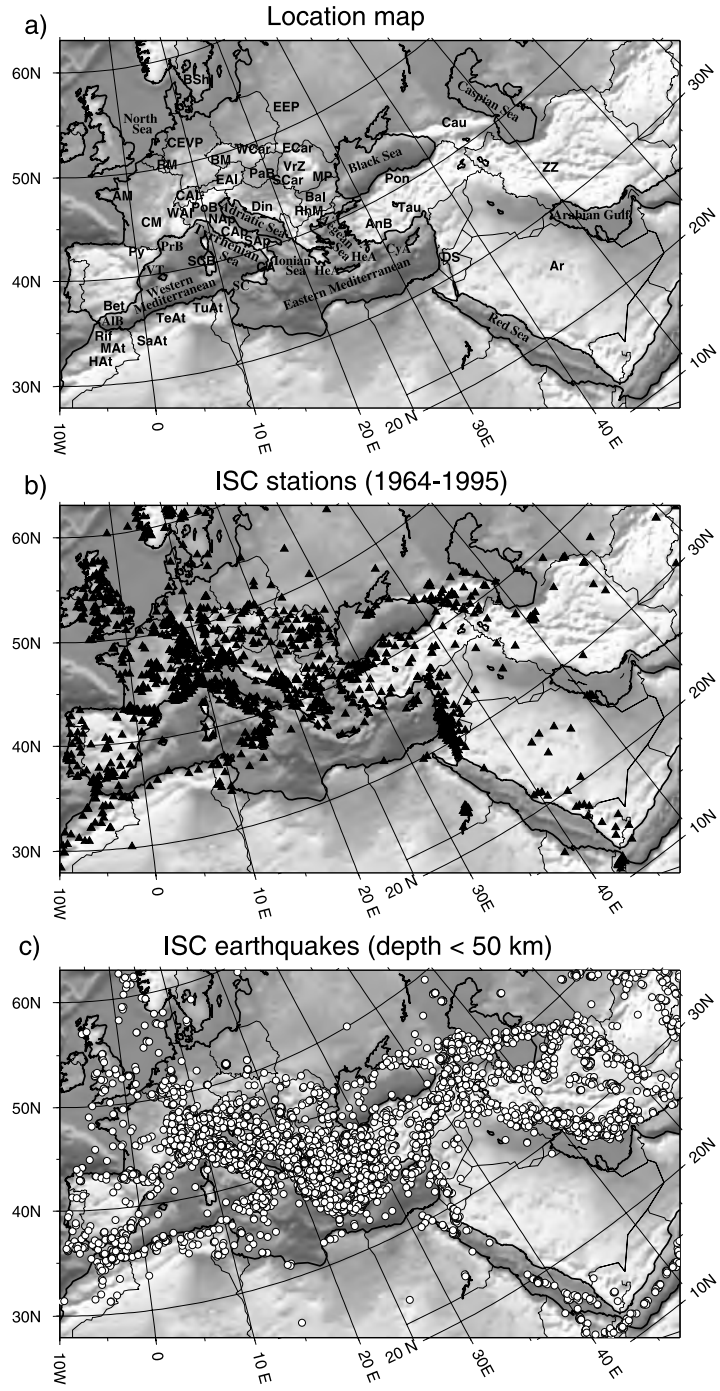

Figure 1. (a) Location map of the Euro-Mediterranean region and nomenclature of the main tectonic units here referred to. AnB = Antalya Basin, AlB = Alboran Basin, AM = Armorican Massif, Ar = Arabian Plate, Bal = Balcans, Bet = Betics, BM = Bohemian Massif, BSh = Baltic Shield, CA = Calabrian Arc, CAl = central Alps, CAp = central Apennines, Cau = Caucasus, CM = Massif Central, CyA = Cyprus Arc, DS = Dead Sea, EAl = eastern Alps, ECar = eastern Carpathians, EEP = east European platform, HAt = High Atlas, HeA = Hellenic Arc, MAt = Middle Atlas, MP = Moesian Platform, NAp = northern Apennines, PaB = Pannonian Basin, PoB = Po Basin, Pon = Pontides, PrB = Provençal Basin, Py = Pyrenees, RhM = Rhodope Massif, Rif = Rif, RM = Rhenish Massif, SAp = southern Apennines, SaAt = Saharian Atlas, SC = Sicily Channel, SCar = southern Carpathians, SCB = Sardinia-Corse Block, Tau = Taurides, TeAt = Tell Atlas, TuAt = Tunisian Atlas, VrZ = Vrancea Zone, VT = Valencia Trough, WA = western Alps, WCar = western Carpathians, ZZ = Zagros Zone. (b) ISC seismic stations location inside the Euro-Mediterranean area. (c) Shallow, $h \leq 50$ km, earthquake epicenters from ISC Bulletin data (1964–1995) after relocation in *sp6* reference model (see text for details). Oblique cylindrical projection centered at 10°W, 45°N with pole at 170°E, 45°N is used.

sional episode driven by the retreat of the Calabrian trench [*Malinverno and Ryan*, 1986]. To date, oceanic space is still present within the collisional belt, both in terms of recently formed oceanic crust (Algero-Provençal Basin and Tyrrhenian Basin) and of oceanic remnants of Mesozoic age (eastern Mediterranean) [*Horvath and Berckhemer*, 1982]. Subduction of this old lithosphere is still occurring below the Calabrian and Hellenic Arcs.

[3] Seismic tomography developed in the last two decades to map the three-dimensional (3-D) heterogeneous velocity structure of the Earth's interior. Through tomography on a regional and global scale, seismology is able to provide useful information to answer questions of geodynamics and tectonics. Indeed, tomography yields more realistic estimates of the amount of subducted lithosphere than seismicity alone can do, detects possible upwellings of hot (low velocity) material from different depths in the mantle, images roots of orogens and allows to argue about the style of convection. The Alpine-Mediterranean area is a wide and complex geophysical laboratory where many questions regarding these topics are still open. In fact, numerous studies appeared in the literature with the goal of imaging the mantle compressional and shear velocity structure of the area, from scales ranging from regional to local, using different methods and data. On a regional scale, *P* wave velocity structure has been studied for example by *Romanowicz* [1980], *Hovland et al.* [1981], *Granet and Trampert* [1989], *Spakman* [1991], *Spakman et al.* [1993], *Piromallo and Morelli* [1997], and *Bijwaard et al.* [1998]. *S* wave velocity structure was revealed through inversion of surface wave phase or group velocities by *Panza et al.* [1980], *Calcagnile and Panza* [1990], *Ritzwoller and Levshin* [1998], and *Curtis et al.* [1998] and through waveform inversion of surface waves by *Snieder* [1988] and body and surface waves [*Zielhuis and Nolet*, 1994; *Marquering and Snieder*, 1996]. Tomographic studies of the lithosphere–mantle structure of smaller areas exploited data from local networks or temporary deployments of arrays: in the Betic-Alboran region [*Blanco and Spakman*, 1993; *Seber et al.*, 1996a, 1996b; *Calvert et al.*, 2000], in the ECRIS [*Glahn et al.*, 1993; *Granet et al.*, 1995; *Ritter et al.*, 2001], in the Italian peninsula [*Panza and Mueller*, 1979; *Babuska et al.*, 1990; *Amato et al.*, 1993; *Selvaggi and Chiarabba*, 1995; *Solarino et al.*, 1996; *Lucente et al.*, 1999], in the Carpathian region [*Fan et al.*, 1998; *Wenzel et al.*, 1998], and in the Hellenic-Aegean area [*Ligdas and Main*, 1991; *Papazachos et al.*, 1995; *Papazachos and Nolet*, 1997; *Tiberi et al.*, 2000]. Though local studies can obtain an extremely good resolution, they are however limited in depth and to small geographical areas, thus hindering sometimes a comprehensive image of the deep structure.

[4] These studies show that the complex tectonic structure of the region is reflected on the heterogeneous distribution of seismic velocities in the lithospheric and sublithospheric mantle. Finer detail is usually revealed by tomographic modeling of the travel times of *P* waves, characterized by high resolution because of wide data availability and because of the short wavelength. *Roecker et al.* [1993] and *Spakman et al.* [1993] suggested the importance of the joint inversion of local/regional and teleseismic travel times to reach better vertical resolution in upper mantle structure. In a previous tomographic study [*Piromallo and Morelli*, 1997], using data from the Bulletins of the International Seismological Centre (ISC), we proposed a different, finer, parameterization and a different processing scheme with respect to those adopted until then. Our results yielded a preliminary model for 3-D *P* wave velocity heterogeneities, which will be referred to as PM97P hereafter. In the present work the investigated volume is broadened both in horizontal and vertical dimensions, and the grid of nodes over which the model is defined has a different orientation to get an improved regional distance ray coverage in the central and eastern part of the model. The model reaches 1000 km depth (300 km deeper than the previous model PM97P), thus improving the ray sampling, not only at depth. Six years of additional data (1990–1995) with respect to PM97P are used. A new scheme to correct teleseismic data for global mantle structure is introduced.

[5] This paper presents the new model, and a discussion of resolution and robustness of its main features. We first describe the data and the method, then the ability of our data to image test structures at different spatial wavelengths, and we finally illustrate the tomographic model with horizontal maps at different depths, and vertical cross sections sliced through selected areas. We provide a discussion of our results and a comparative analysis both on a large and small scale, although a detailed presentation and interpretation of the tomographic model in terms of tectonics and geodynamics is out of the scope of this paper and will be given elsewhere.

2. Data Selection and Earthquake Relocation

[6] The convoluted tectonic setting of the Mediterranean region originates a complex pattern of seismic activity. Seismicity is characterized by the occurrence of frequent low to moderate magnitude events, and occasional large magnitude earthquakes. As illustrated in Figure 1c, the most active areas are interplate regions located at the margins between the main interacting plates (Africa, Eurasia, and Arabia) and microplates (Anatolia and Iberia) of the Mediterranean domain. However, intraplate shallow seismicity is also present. Shallow earthquakes have a rather uniform distribution over the area (Figure 1c). Deep and intermediate-depth events are instead clustered in the Hellenic Arc (depth $\leq$180 km), Cyprus Arc (depth $\leq$130 km), Calabrian Arc (depth $\leq$500 km), Betic-Rif (depth $\leq$160 km and three isolated events at $\sim$600 km depth), and eastern Carpathians (depth $\leq$220 km). The pattern of both shallow seismicity (Figure 1c) and station distribution in the area (Figure 1b) justifies our choice for the volume to be investigated. We define the cell model with a regular spacing in a coordinate system rotated with respect to the geographical one, as given by an oblique cylindrical projection, centered at (10°W, 45°N) with pole at (170°E, 45°N). This choice is intended to have the model area lying astride the new Equator, which allows to obtain cells of approximately the same size in both directions. The model horizontal dimensions are 6600 km in E-W direction, 3900 km in N-S direction, approximately, and 1000 km in depth. The orientation and aspect ratio of the volume allow to optimize the sampling by regional rays.

[7] *P* wave travel times reported by the ISC for the time period 1964–1995 constitute our data set for the present work [*International Seismological Centre*, 1997]. During

the six additional years with respect to the data set used in PM97P a significant number of new stations have been deployed throughout the Mediterranean, highly improving coverage in some key areas (i.e., Morocco, Tunisia, Syria, and Turkey). This study will benefit by a good ray sampling especially in the central and western Mediterranean Basin. The extreme paucity, or lack, of stations in the central eastern part of the North African margin does not instead allow a satisfactory illumination below the eastern Mediterranean basins (see Figure 1b).

[8] Earthquakes are carefully selected on the basis of a few simple but stringent criteria, meant to sort out only the well recorded ones. Each event is required to have the following characteristics: (1) a shallow hypocentral depth ($\leq$50 km), (2) at least 30 first arrivals reported by stations at regional or teleseismic distance, and (3) a largest open azimuth of no more than 2 over 8 adjacent azimuthal sectors (in the worst case it can be close to 180°). Application of these selection criteria limits location bias due to uneven ray path distribution and ensures more homogeneity in earthquake geographical distribution and path coverage; intermediate-depth and deep earthquakes are rejected because they are heavily clustered in small volumes. Focal depth is not always very reliable in bulletin data [e.g., *Engdahl et al.*, 1998]. However, as we only use shallow hypocenters, this is not expected to have an appreciable effect on our model because direct P first arrivals are in fact rather insensitive to source depth (due to trade-off with origin time). For all analyses, we only retain arrivals in the epicentral distance range $3° \leq \Delta \leq 90°$ to avoid crustal *Pg* arrivals and core–mantle boundary diffractions.

[9] The ISC Bulletin is the most widely used data set for travel time tomography at this wide scale, since it includes a large number of earthquakes and stations, and a massive collection of arrival times. It is a rather heterogeneous data set (varied instrumentation and technology for data acquisition, different analysts, and picking procedures). Its arrival times are affected by random and systematic sources of errors and data quality may vary significantly [i.e., *Grand*, 1990; *Gudmundsson et al.*, 1990; *Röhm et al.*, 1999]. In spite of this, ISC data set is the one with the highest possible resolution for this kind of studies.

[10] We process all selected earthquakes, relocating them using the radial global Earth model *sp6* [*Morelli and Dziewonski*, 1993], to remove the systematic bias in hypocentral parameters due to the ISC location procedure based on JB travel time tables [*Jeffreys and Bullen*, 1940]. The location is performed by means of an iterative least squares optimization of first arrival residuals. Initial residuals are calculated using hypocenters and arrival times given by the ISC reports, and travel times computed in the *sp6* model. Each first arriving phase is always associated to the theoretical first arrival at that distance. *Pn* arrivals follow the same association criterion as the other first arrivals, regardless of any identifier reported in the ISC data set. Tables of travel times as a function of slowness are interpolated using the τ-spline method [*Buland and Chapman*, 1983] to find the theoretical travel time for the reference model at any given epicentral distance. Source depth is fixed and standard corrections such as for ellipticity [*Dziewonski and Gilbert*, 1976] and station elevation are applied.

[11] Worldwide available first arrival P phases, at teleseismic and regional distance, are used to locate the events. The procedure adjusts origin time and epicentral coordinates to minimize the summed squared weighted residuals for each event, following the uniform reduction scheme [*Jeffreys*, 1932], with average distribution parameters appropriate for regional and teleseismic *P* residuals [*Piromallo and Morelli*, 1998, 2001]. Event mislocations can be computed with respect to a selected set of ground-truth test events [*Piromallo and Morelli*, 2001]. Root-mean-square (RMS) difference between known hypocentral parameters and those found after 1-D location in *sp6* model is 16.39 km for earthquakes and 9.95 km for explosions recorded at teleseismic distance. RMS values of this magnitude, which are an improvement with respect to the bulletin estimates, represent the largest advancement that can be attained using just a 1-D reference Earth model. The effects of relocation in *sp6* and in a heterogeneous Earth are specifically addressed by *Piromallo and Morelli* [1998, 2001].

[12] We locate over 52,000 selected events using more than 5,000,000 observations. All rays having either source or receiver in the study area, are then stored for subsequent use.

3. Tomographic Method

3.1. Summary Rays and Static Corrections

[13] Summary residuals are often used, rather than individual observations, as input data to the inversion because summary rays reduce spatial imbalance in data coverage, they minimize noise related to small-scale crustal heterogeneities, and they limit the redundancy of data in the inversion, at the same time retaining the geographically dependent character of travel times [i.e., *Morelli and Dziewonski*, 1991; *Robertson and Woodhouse*, 1995]. To compute summary residuals the Earth's surface is subdivided in cells and all individual rays connecting the same pair of cells, regardless of which of the two contains the source and which the receiver, are grouped into a summary ray. To this purpose, we use two nested grids: 1656 approximately equi-areal trapezoidal cells on the whole globe (cell size is $5° \times 5°$ at the Equator), and 8400 smaller cells ($0.5° \times 0.5°$) in the Mediterranean area. Summary rays therefore stem from each cell of the target area containing stations, events, or both. This strategy increases the coverage with respect to studies based only on rays travelling to stations inside the area. To each summary ray a residual is then associated, defined as the weighted average of all individual residuals contained in the bundle [*Piromallo and Morelli*, 2001], where the data weighting function is the uniform reduction weight specified by *Jeffreys* [1932].

[14] Residuals of regional distance summary rays ($\Delta \leq 28°$) are used in the inversion only if they travel entirely within the volume, in order to prevent mapping of lateral heterogeneities close, but external, to the inversion domain into our model. Moreover, only summary rays with residual less than 3 s, and composed by at least 3 individual observations, are retained as input to the inversion. This procedure and further selection isolate a total of 112,139 (52,514 regional and 59,625 teleseismic) summary rays, out of 334,723. The RMS reduction of residuals due to sum-

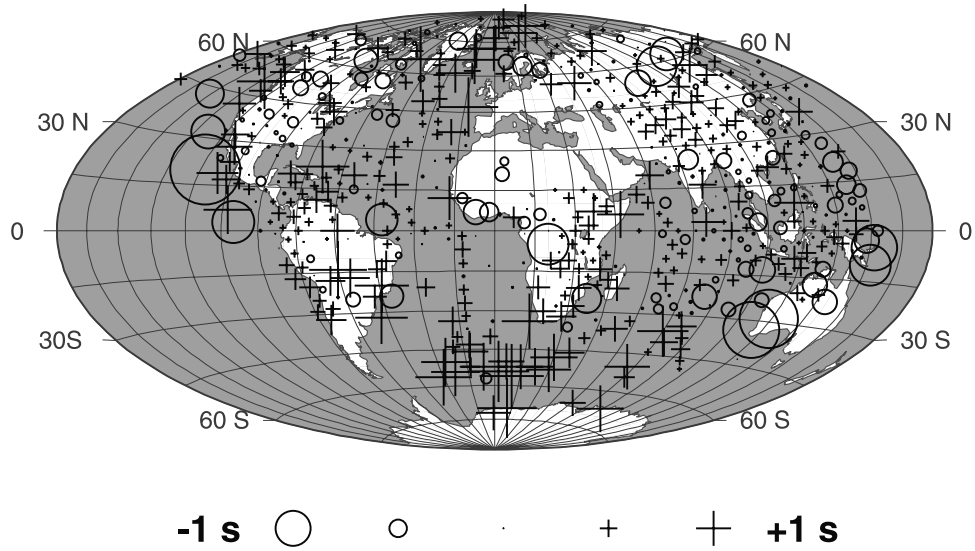

Figure 2. Mantle corrections computed for roughly equal area 5° × 5° cells used to account for aspherical velocity structure outside the model volume. Pluses and circles indicate positive and negative corrections, respectively. Each correction is obtained through a selective sampling of the mantle by paths travelling to the Mediterranean from a cell located at teleseismic distance outside the investigated region (see text for details).

mary ray formation before inversion is about 31%, the initial RMS being 1.44 s.

[15] Due to the large-scale character of this study, ray paths of teleseismic observations do not entirely lay within the model volume, thus providing a sampling of both the target volume and of the mantle heterogeneities located outside. An erroneous mapping of these anomalies into our model may occur, unless we apply an appropriate correction for teleseismic data. To this purpose, regional tomographic studies often use station static corrections, either as model parameters in a joint inversion for the 3-D velocity structure [e.g., *Spakman et al.*, 1993] or as independent parameters in a stepwise sequence [e.g., *Calvert et al.*, 2000]. Other studies reduce the effect of outside structure by embedding their regional model in a global (more coarsely parameterized) mesh [*Fukao et al.*, 1992; *Widiyantoro and van der Hilst*, 1996] or by doing global inversions with an adaptive grid to achieve high resolution locally [*Bijwaard et al.*, 1998; *Sambridge and Gudmunsson*, 1998; *Kárason and van der Hilst*, 2001].

[16] We follow a different approach and devise a scheme which allows the use of teleseismic rays, by introducing a straightforward alternative to a global inversion to correct for structure outside the model volume. For each 5° × 5° cell of our global grid, we estimate the contribution of the external mantle structure to the total delay, by averaging all summary residuals from summary rays connecting that cell to any small cell in the Alpine-Mediterranean region. Our mantle corrections represent a path-integrated account of large-scale velocity structure, as a result of a selective sampling of the mantle in the ''fat beam'' based on the 5° × 5° cell, on one end, and the 35° × 60° base of the model volume, on the other end. This is better than using static teleseismic station corrections, which instead give a global sampling of the whole mantle as seen from each station. In addition, our reciprocal summary rays, combining sources and stations in each cell, permit the calculation for several more cells at teleseismic distance.

[17] Mantle corrections are plotted in Figure 2. Analogously to station statics [e.g., *Robertson and Woodhouse*, 1997] our selective mantle corrections represent a first approximation account of large-scale mantle velocity structure. Each correction, shown in Figure 2, is the result of a selective sampling of the mantle by paths travelling from, or to, the Mediterranean, and therefore represents the contributions of long-wavelength lower mantle structure, and shorter-wavelength (∼5°) upper mantle structure outside the model volume. Some general features of these mantle corrections are nonetheless similar to classic station statics [*Dziewonski and Anderson*, 1983; *Hager and Clayton*, 1989; *Zhou and Wang*, 1994] insofar they are correlated with lithospheric structure beneath the remote receiver or cell: negative delays therefore mark shield areas, and positive delays are present in younger tectonically active continental regions, and across ocean ridges and rifting areas. The mantle corrections range from −2.9 to +4.2 s, with RMS 0.64 s and average 0.24 s. This positive regional average is a consequence of the upper mantle beneath the Mediterranean being slower than the global reference, and has no effect for our goal of reconstructing lateral variations of velocity, but should be taken into account if absolute velocities are sought. For scarcely populated cells, up to about 10 summary rays, the norm of regionally averaged cell terms decreases as the number of summary rays increases [*Piromallo and Morelli*, 2001], but this effect is not crucial for more populated cells.

3.2. Parameterization and Inversion

[18] We parameterize the perturbation of the slowness field by means of local basis functions, represented by 3-D linear splines on a 3-D lattice of 180,411 nodes (121 and

71 nodes, respectively, in the EW and NS direction, 21 nodes in depth). The horizontal spacing is again 0.5° in both horizontal directions, while the vertical spacing is 50 km. In general, the use of a continuous interpolator gives a more realistic description of the velocity field, if compared to a block-wise model with the same number of parameters [*Nolet*, 1996]. Travel times of *P* waves, with period of the order of 1 s and wavelength of about 10 km in the mantle, are able to resolve structures of 30–80 km wavelength at upper mantle depths and of 100–200 km at lower mantle depths [*Nolet*, 2000]. Our parameterization, with node interspacing of about 55 km, is thus potentially suitable for describing features not smaller than this size. Of course, structures are not necessarily resolved to the block size (nominal resolution), as will be explained in the next section. Moreover, the station and event distribution in the Alpine-Mediterranean region (some of the 0.5° × 0.5° squares may not even contain any seismographic station or earthquake), may map shorter-wavelength structure into a larger-scale, smoother model, and hence introduce some artifacts in the upper layers in correspondence of these scarcely sampled areas. However, a fine grid is the best measure we can take to limit this aliasing effect.

[19] The forward problem is solved by 1-D ray tracing through a ray shooting algorithm in spherical geometry in *sp6* background model. *Pn* ray paths result analytically as the effect of refraction at the 35 km deep Moho. In the area encompassed by this study, velocity anomalies rarely exceed a few percent, so that 1-D ray tracing can be considered a legitimate approximation. The use of a 1-D ray tracing algorithm may have a smoothing effect on the resulting model of a strongly heterogeneous region of the upper mantle. A rough estimate of this smoothing effect is given by *Bijwaard and Spakman* [2000, Figure 3a]. Differences in RMS amplitudes between models resulting after 3-D or 1-D ray tracing are of the order of 0.2% in the crustal layer (35 km) and attain a maximum 0.5% in the lithospheric layers (70,120 km), below which they become negligible.

[20] The solution to the inverse problem is sought by least squares minimization through the iterative LSQR algorithm [*Paige and Saunders*, 1982; *Nolet*, 1987]. Though LSQR is intrinsically damped, we introduce an additional explicit roughness damping through an isotropic gradient minimization condition, to constrain ill-determined model parameters. We assume that observational errors are Gaussian and uncorrelated, with standard deviation 1 s, and we assign an a priori probability density distribution for the change of seismic velocity between any couple of adjacent nodes shaped as a Gaussian with zero mean and standard deviation 0.5%. The gradient constraint is applied both horizontally and vertically; only the top layer (at 0 km depth) is kept unconstrained, in order to limit the contamination of the layer below (at 50 km depth) by unmodeled crustal heterogeneities. The overall regularization applied is thus a combination of norm and gradient damping, isotropic and without any depth dependence.

[21] Our *P* velocity model PM0.5 is obtained after 15 iterations of the LSQR algorithm. The RMS reduction in the residuals due to data fit in the inversion is about 26%, comparable to 28% obtained by *Spakman et al.* [1993].

4. Sensitivity Analyses

[22] Ray paths provide a rather inhomogeneous illumination of the mantle structure. Before inspecting the results of the inversion, it is therefore important to analyze the path distribution over the model volume. Figure 3 depicts, in map view and logarithmic scale, the ray density for some layers of the model. Ray density is the cumulative value of the partial derivative of slowness with respect to travel time, a quantity analogous to the cell hit-count in studies based on block parameterization.

[23] The consequence of the inhomogeneous distribution of seismicity and stations in this area on ray illumination is clearly seen from a comparison of Figure 3 with Figures 1b and 1c. There is substantial difference, especially in the shallower layers, in the coverage provided by teleseismic rays, confined to areas right below stations and events, and regional rays, more extensively sampling the regions in between the ray foci. In fact, the 50 km depth layer is largely dominated by horizontally travelling *Pn* rays, sampling the lithosphere and crossed by vertical teleseismic rays in correspondence of stations and events (which give the spot-like features in some regions). Earthquakes in the Hellenic-Aegean region, recorded by European stations, provide an extremely good coverage of the central western part of the model, although most rays have a SE-NW trend. At 150 km, the ray coverage is more uniform, but the maximum density is lower than above. In both layers, the coverage of the African margin, the eastern European platform, and the Arabian Plate is limited to small areas, unevenly sampled, due to sparse station and event locations and to the location of these regions in the periphery of the domain. At intermediate depths (250 km) the illumination gaps in these regions are partially filled by incoming teleseismic rays, and we observe a more uniform ray density all over the area. This is even more evident moving from 350 to 450 km depth, with the fairly illuminated area extending northward and eastward. Moving to deeper layers (600–700 km) ray sampling gradually extends to the border of the region, practically achieving a full coverage of the area by teleseismic rays in the lowermost 200 km. An enhanced sampling in the layer below each discontinuity (450 and 700 km) can be noticed, due to the refraction at the interfaces of regional rays and subsequent subhorizontal sampling.

[24] In the case of a manageable number of parameters, the best way to assess the reliability of the estimated model is to compute the full resolution matrix, which contains the whole information, and the a posteriori error matrix. When we are faced with an very large number of unknowns, presenting a readable matrix is however a problem. We can alternatively resort to "sensitivity tests" [e.g., *Spakman and Nolet*, 1988; *van der Hilst and Engdahl*, 1991; *van der Hilst et al.*, 1993; *Lévêque et al.*, 1993], which address the resolution of the inversion scheme in terms of its ability to retrieve a known input model, given the same ray coverage which will be used for the real data inversion. Sensitivity analyses allow for a comprehensive, relatively rapid, visual inspection in the spatial resolution of a model

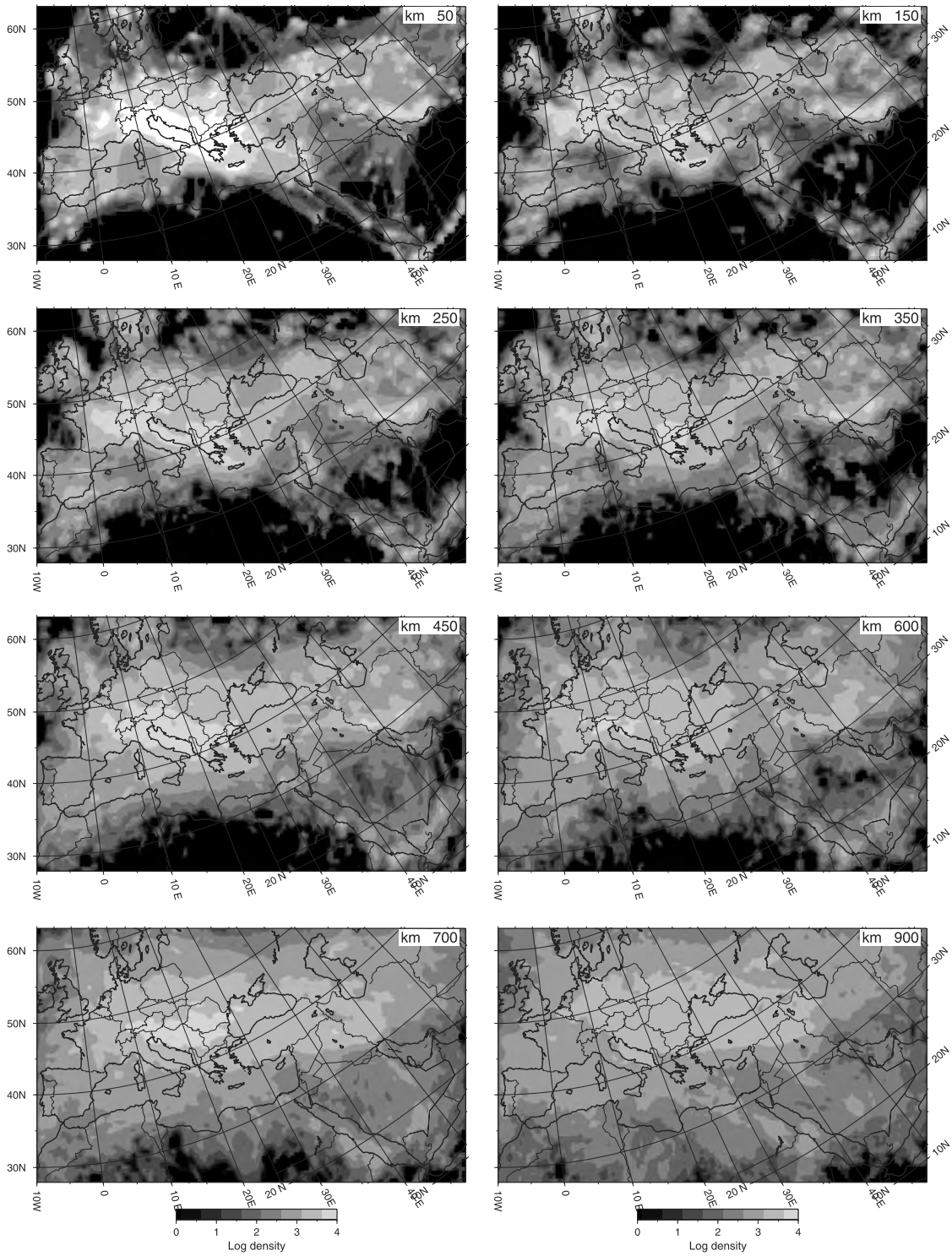

Figure 3. Ray density (cumulative value of the partial derivative of slowness with respect to travel time) distribution in a logarithmic scale. The ray density field does not vary rapidly with depth. Therefore, we only display maps located at representative depths: two shallow layers (50 and 150 km), an intermediate one (250 km), one layer above and one below each upper mantle seismic discontinuity (350, 450, 600, and 700 km), and one in proximity of the base of the model (900 km). Solid black is used for regions of no sampling. See text for comments.

with a large number of parameters, provided that the assumptions made hold true. However, they only provide qualitative estimates of accuracy and resolution, and they only show a limited representation of the resolution matrix. The synthetic travel times used to retrieve a sample structure are computed with the same theoretical apparatus, and simplifications, that are used for the actual inversion, and do not therefore test the effect of ''errors'' in the theory.

Table 1. Parameters and Characteristics of the LSQR Inversion of Real Data and Synthetic Models[a]

	Input Anomaly			RMS of Residuals		
Model	Length (km)	Amplitude (%)	σ (s)	Before (s)	After (s)	Reduction (%)
Real data	–	–	–	0.99	0.73	26
chess 1	∼110	4	0.85	0.85	0.72	14
chess 2	∼200	4	0.85	0.85	0.72	14
harmo 1	∼300	4	0.85	0.99	0.72	27
harmo 2	∼600	4	0.85	1.18	0.72	39
impulse	∼110	7	0.40	0.63	0.52	17

[a]The size and amplitude of the input velocity anomalies for the sensitivity tests are specified together with the standard deviation of the Gaussian noise (σ). The damping parameter and the number of iterations in the inversion are always the same as for the data inversion. The RMS values of residuals before and after inversion are listed together with the RMS reduction in percent, both for the real data and for the synthetic models.

Furthermore, only specific features (e.g., chessboard and harmonic fields) can be used, and therefore only sensitivity to those particular shapes, very different from the real Earth structure, can really be addressed [*Lévêque et al.*, 1993]. In spite of these shortcomings, sensitivity tests have become a standard way of addressing model resolution as their results can be promptly visualized.

[25] We perform several synthetic tests, in order to study the resolution for patterns of long, intermediate and short wavelengths of geodynamical interest and for sharp or smooth anomaly contrasts. The input synthetic models are constructed as regular patterns of velocity variations relative to the surrounding reference velocity profile. Travel times are then computed by forward calculation through the synthetic model, and Gaussian random noise, with standard deviation σ, is added to the data before inversion. The value of σ for the Gaussian noise is chosen to approximately reproduce the signal-to-noise ratio of the actual data, as explained in detail by *Piromallo and Morelli* [1998]. The same inversion parameters as for actual data are then applied, i.e., number of iterations and regularization. Their values are reported in Table 1, together with the variance reduction obtained in the inversion for each test and for the real data.

[26] We show here the results of chessboard tests where input heterogeneities of alternating sign (±4%) are superimposed on the ambient velocity profile. The positive/negative anomaly is attributed to the same number of nodes in each direction, separated by an equal number of zero amplitude anomaly nodes. Gaussian random noise, with standard deviation σ = 0.85 s, is added to the data. Different wavelength patterns are tested, among which we show two representative results. The first test, in the left panels of Figure 4, is aimed at estimating retrieval of small-scale structures (boxcar anomalies of two nodes in each direction, approximately 110 km in size). Horizontal smearing of anomalies of this size occurs in regions where ray sampling is poor and/or strongly anisotropic. All over the depth range of the model this effect is particularly pronounced in the Red Sea, Arabian Plate, and eastern European platform, sometimes even joining the anomalies over several nodes. In the Northern African margin, the western and eastern Mediterranean, northern Europe, Black Sea, eastern Turkey, Caucasus and Zagros region smearing is still present but less critical. In the remaining regions, small-scale heterogeneities are satisfactorily retrieved in the depth range sampled by both regional and teleseismic rays, while their amplitude decays in the lowermost 200 km of the model. Vertical leaking of anomalies is confined to the closest layer in areas of good sampling and at shallow depths. In each layer, amplitudes of the anomalies are strongly dependent on the ray density, as may be expected. In the right panels of Figure 4, larger-scale structures (four-node anomalies, approximately 220 km, in each direction) are analyzed. With respect to the previous pattern, this is more easily retrievable in amplitude, and the area over which reliable images are obtained is enlarged horizontally and extends to the bottom of the model (though some noise distorts the shape of the input model). For example also the western Mediterranean, Northern African margin, Black Sea, Turkey, Caucasus, and Zagros region are nicely retrieved. Moving to the deeper layers, the area of recovered features extends to the north, NE, but the portion of Africa and Arabian plate still remains unresolved or highly smeared.

[27] We also did a harmonic model recovery test. The input pattern is given by 2-D smoothly varying features, obtained by superposition of sine functions, with amplitudes ranging between ±4% and delay times are again contaminated by Gaussian random noise before inversion (see Table 1). Wavelengths of ∼300 and ∼600 km in both horizontal directions are considered. Figure 5 shows the RMS amplitude of both retrieved models (lengths ∼300 and ∼600 km) and of the input model, as a function of depth. The RMS profiles indicate that retrieved amplitudes are rather uniform with respect to depth, the only exceptions being at the top and bottom of the model. The amplitude of the layer at 50 km depth is better recovered, due to the strong sampling provided by Pn rays. The two extremal layers, at 0 and 1000 km, have instead lower amplitudes, a geometric effect due to the lower sampling provided by rays to the nodes located at the boundaries of the inversion volume (only the ray segments inside the volume are considered). The layer at 0 km is also affected by a more irregular sampling, due to ray clustering at stations and hypocentral areas. The RMS amplitudes of the reconstructed model are about 60% of the input pattern, larger for broader anomalies.

5. Main Features of Model PM0.5

[28] For sake of completeness, and to preserve the 3-D continuity of its features, the resulting model is displayed in its totality, by means of map views at all the different depth levels. Model PM0.5 is expressed as percentage velocity perturbation with respect to the reference model *sp6*. The average anomaly over a horizontal layer is always subtracted for clarity. Layer averages are shown in Figure 6 as a function of depth. Since the values are always rather small, less than 0.2%, the new average P velocity profile is almost undistinguishable from the background model *sp6*.

[29] An overall decreasing structural complexity and amplitude weakening is observed moving from the surface to depth, since the Earth structure is particularly heterogeneous with strong regional variations in the uppermost 250 km. This is clearly illustrated by Figure 7a, where we show the RMS amplitude of model PM0.5 and of separate test inversions of teleseismic and regional data, plotted as a

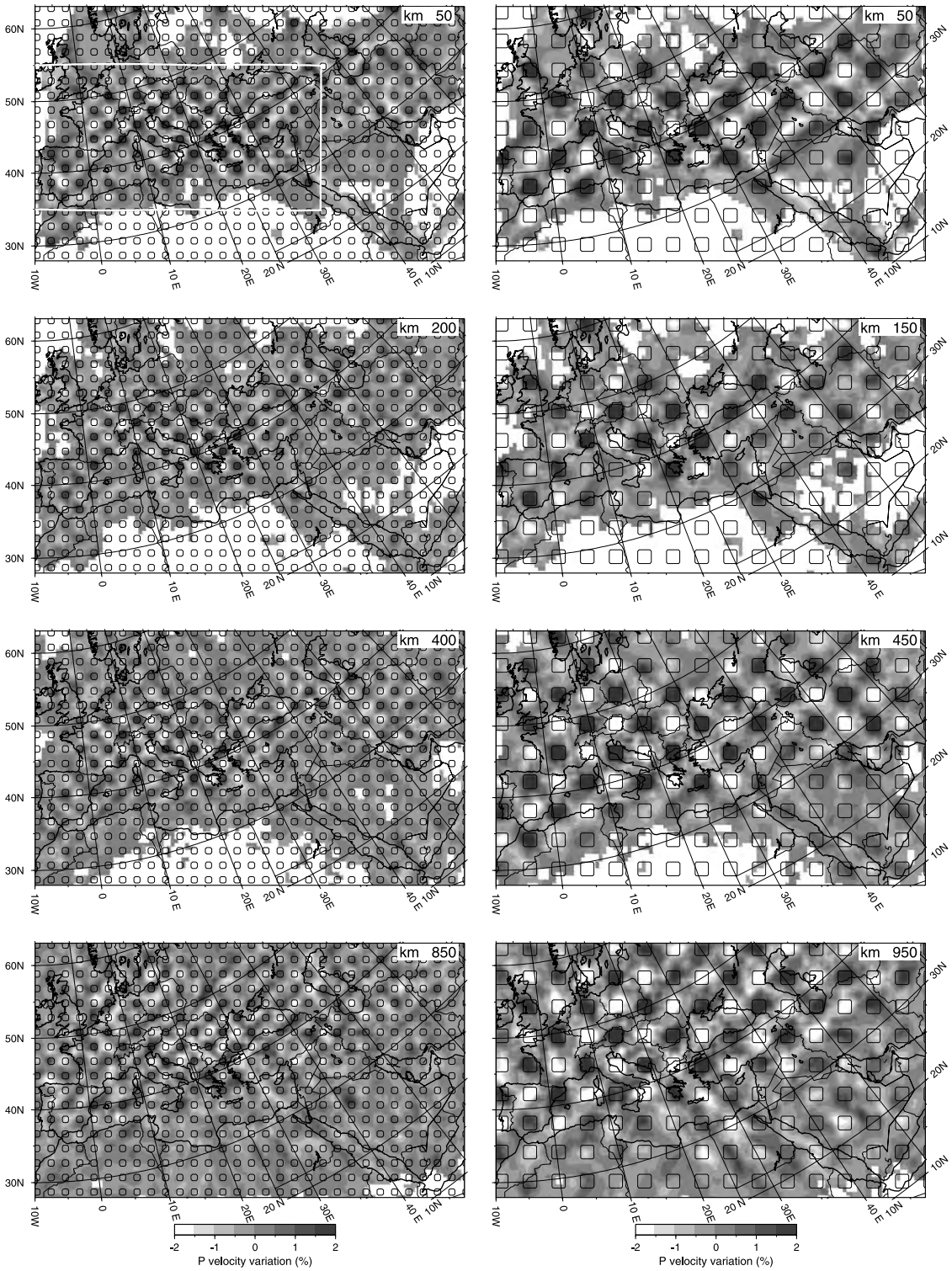

Figure 4. Chessboard recovery test in map views at some selected depths. Input heterogeneities of opposite sign (whose location is indicated by ±2% contouring) are alternately superimposed on the ambient velocity profile and are marked by contouring. The input anomaly is attributed to the same number of nodes (2 nodes in the left panels, 4 nodes in the right ones) in each direction, separated by an equal number of unperturbed nodes. Gaussian random noise is added to the data before inversion. The output model is given in gray shades. The rectangle in the top left panel identifies the region best resolved at all scale lengths.

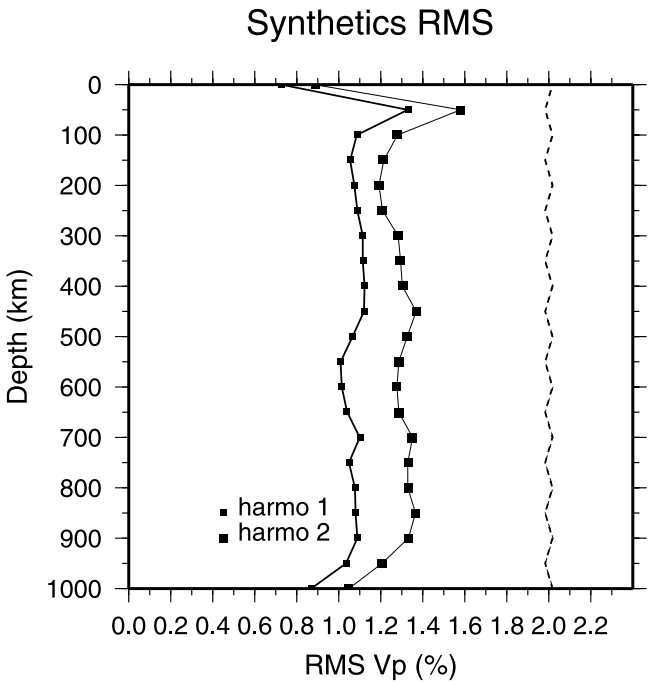

Figure 5. RMS amplitude as a function of depth for harmonic sensitivity tests. The input pattern of the harmonic models is given by the superposition, in each layer, of sine functions in the two orthogonal directions, giving a 2-D harmonic slowness anomaly pattern, with amplitudes ranging ±4% and characteristic lengths of ∼300 and ∼600 km. Delay times are contaminated with Gaussian random noise (Table 1). The retrieved harmonic models for anomalies of ∼300 km (harmo 1) and ∼600 km (harmo 2) size are shown together with the RMS amplitude of the input model (dashed line). RMS amplitudes are computed within the best resolved region of the model shown in Figure 4 (top left panel).

function of depth. Comparison with Figure 5, showing instead that input patterns are retrieved with rather uniform RMS amplitudes, indicates that the behavior of Figure 7a is not an artifact of ray sampling. Overall, model RMS amplitudes decrease rapidly going from the shallow part of the model to larger depth [see also *Fukao et al.*, 2001]. The transition zone is marked by a relative increase of RMS amplitudes, mainly retrieved by regional rays. Although characterized by smaller-depth sensitivity, teleseismic rays detect the decrease of RMS amplitude with depth, and obviously contribute the most to constrain the model at larger depths. In Figure 7b we show instead the relative contribution of positive and negative velocity anomalies to the RMS amplitude of PM0.5. At shallow depths (≤250 km) slow anomalies have slightly larger RMS amplitudes than fast ones. Below 250 km, instead, fast anomalies have larger RMS amplitudes than slow ones, sensibly higher in the transition zone, less pronounced in the shallowest lower mantle. High RMS amplitude in the transition zone are only present in positive anomalies.

[30] Each map in Figure 8 reports relative *P* velocity variations on the horizontal layer of the 3-D grid at that depth. Some selected vertical cross sections, obtained from the 3-D model with average velocity profile subtracted, are shown in Figure 9, along with the ray density distribution and an impulse recovery test (two-node input anomalies by ±7% in each direction, separated by six unperturbed nodes, see Table 1). Additional material can be found on the Web site (http://www.ingv.it/seismoglo/ptomo).

[31] The "crustal" layer at 0 km depth is shown but it is not interpreted since it suffers from the strongly inhomogeneous distribution of stations and events, the effects of unmodeled shallow structure, and of smearing from the close layer at 50 km. The contribution of regional rays is dominant, amplitudes are very large in well sampled areas and velocity contrasts are quite sharp. This velocity pattern is affected by a trade-off between variations in crustal thickness and velocity anomalies. Since no crustal correction is taken into account, neglected heterogeneities in crustal thickness (with horizontal scales comparable to those of main tectonic features) may induce quite large variations in the travel times of shallow travelling rays. Smaller-scale heterogeneities (less than about 50 km) are instead filtered out by the use of summary rays.

5.1. Large-Scale Features

[32] The most prominent large-scale feature of PM0.5 at shallow depth is the difference in the upper mantle structure between the Precambrian Baltic and east European Shields, marked by high velocities, and the low velocities of the western and central Euro-Mediterranean young tectonic provinces. The high velocity below the east European platform and Baltic shield is continuous in PM0.5 from 50 to 350–400 km, and particularly pronounced in the depth range 100–300 km. The western Mediterranean Basin and Europe are instead overall dominated by slow velocity anomalies between 100 and 400 km depth on a large scale. This pattern of large-scale shallow anomalies is in accord with results from other P and S tomographic models [*Romanowicz*, 1980; *Snieder*, 1988; *Spakman et al.*,

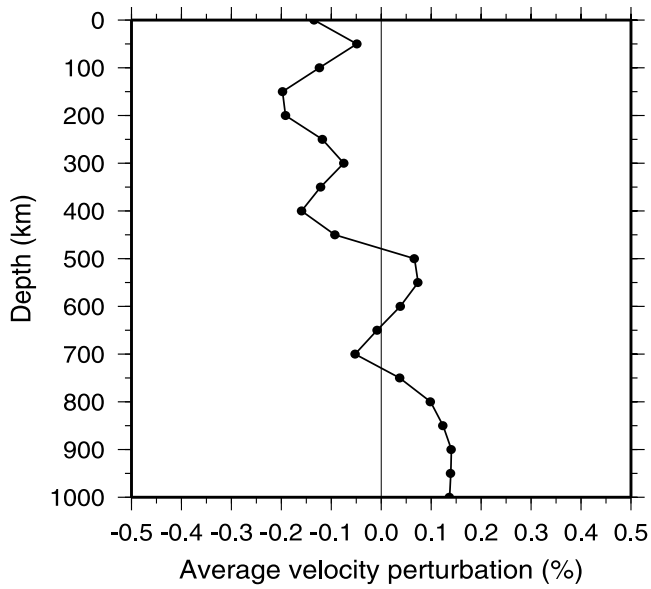

Figure 6. Averages of velocity anomalies over horizontal layers as a function of depth. These values are subtracted, layer by layer, from the model to produce the map views in Figure 8.

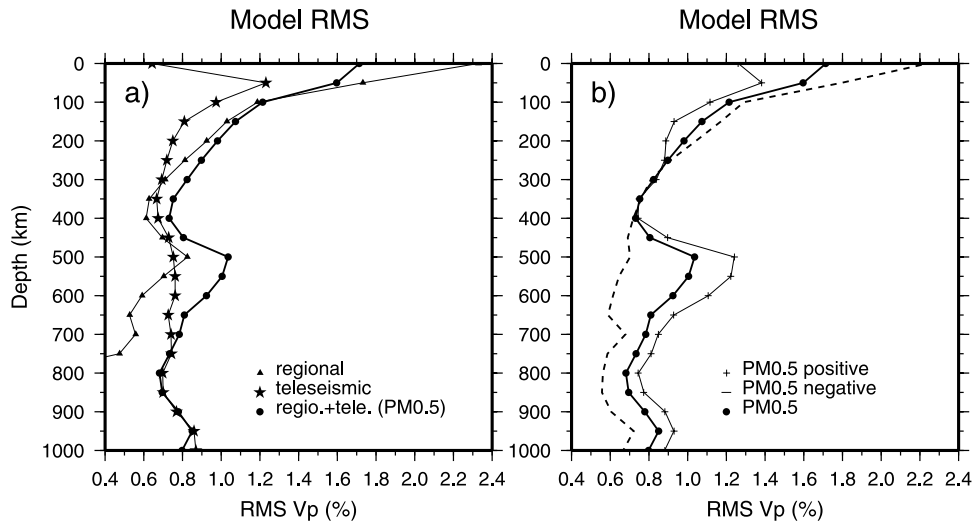

Figure 7. (a) RMS amplitude of model PM0.5 velocity anomalies and of the separated inversions for teleseismic and regional rays only, plotted as a function of depth. (b) RMS amplitude of PM0.5 velocity model, as a function of depth, computed separately for positive (pluses) and negative (dashed line) anomalies. RMS amplitudes are computed within the best resolved domain marked in the left top panel of Figure 4.

1993; *Zielhuis and Nolet*, 1994; *Marquering and Snieder*, 1996; *Curtis et al.*, 1998]. However, in our model the sharp gradient of the boundary between east and central Europe, running along the ancient suture of the Tournquist-Teisseyre zone, extends to depths of at least 300 km, larger than in previous models [*Zielhuis and Nolet*, 1994].

[33] Another dominant feature is the approximately continuous S-shaped fast anomaly that can be followed, through the four layers at 250–450 km depth, from the North African margin, to the Calabrian Arc, the Apennines, the Alps and the Carpathians. It represents the signature of subducted lithosphere along the Alpine collisional belt [*Wortel and Spakman*, 1992; *Spakman et al.*, 1993; *Piromallo and Morelli*, 1997]. In the 500–700 km depth range the ray sampling is clearly more uniform for the whole area, due to the contribution of teleseismic rays. The pattern of fast anomalies of the previous layers joins into a wide and strong high velocity feature, approximately located in the central part of the model. The most remarkable heterogeneity lies beneath the area interested by the Alpine orogeny, the Turkish promontory and, to the east, the Zagros Zone. A large amount of fast velocity material stagnant in the transition zone below Europe [e.g., *Spakman et al.*, 1993; *Marquering and Snieder*, 1996] is particularly evident in PM0.5 (see also cross section Cc, Figure 9), and could be the remnant of the Tethyan oceanic lithosphere.

[34] Only teleseismic rays illuminate the structure below the 670 km discontinuity. At these depths teleseismic rays are not as vertical as in the lithosphere, therefore we do not expect too strong vertical smearing. Two deep large-scale anomalies are present in the 850–1000 km depth range: the slow velocity region under northwestern Europe and the high velocity area from the Ionian Sea to Turkey. The low velocity is part of a broader and deeper slow anomaly possibly related to a lower mantle upwelling [*Goes et al.*, 1999]; the fast velocity anomaly corresponds instead to the westernmost edge of the Tethyan subduction belt [*Grand et al.*, 1997; *van der Hilst and Karason*, 1999; *Faccenna et al.*, 2003]. The bottom layers of the model are the ones most prone to contamination from neighboring, external, Earth structure. The good agreement of our results with whole-mantle models, however, supports the robustness of these features. We regard to this result as to a significant verification of the effectiveness of mantle travel time corrections, and of the reliability of both approaches.

5.2. Small-Scale Features

[35] On a smaller scale, fast velocity anomalies characterize the lithosphere of the basins. Some of them are well confined to the shallowest layer at 50 km (like the western Mediterranean, Adriatic and Ionian Basin), some others propagate to the layer below at 100 km (as Black and Caspian Sea), or even down to 150–200 km (as in the eastern Mediterranean Basin, where however some vertical smearing is likely). Low velocities at these depths mark instead areas of rifting (as the ECRIS, the Sicily Channel, and the Dead Sea), back arc regions (as the Alboran, the Tyrrhenian and the Aegean Sea, and the Pannonian Basin) and magmatic provinces (as the volcanic provinces of central Italy and central Europe). A fast velocity feature, laterally discontinuous, along the North African margin is imaged, though at the border of the illuminated region, gaining amplitude from shallow (50 km) to deeper layers (400 km).

[36] Beneath the Alboran region, seismically slow material at shallow depth (50–150 km) is underlain by a single coherent fast body, SW-NE oriented, apparently continuous from 250 down to 700 km depth. Most of the recent larger-scale seismic tomography studies agree in detecting a large positive anomaly interpreted as the image of a subducted slab [*Spakman et al.*, 1993; *Blanco and Spakman*, 1993; *Piromallo and Morelli*, 1997; *Bijwaard et al.*, 1998]. Our model also reveals significant anomalies in northern Africa, in correspondence of the Rif region, in the 50–150 km depth range (see Figure 8), previously overlooked by larger-

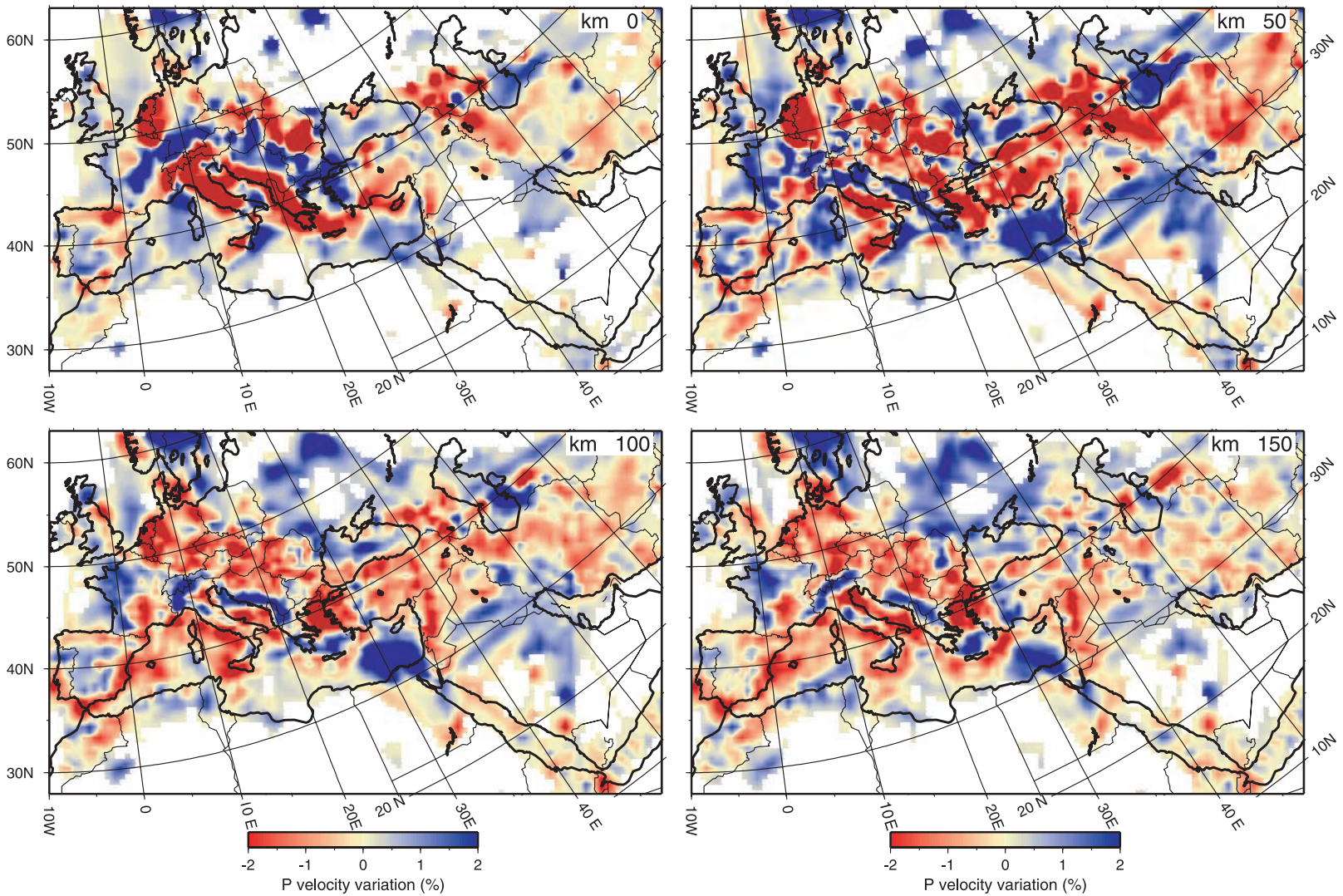

Figure 8. Map views of our best 3-D model PM0.5. *P* velocity perturbation with respect to reference model *sp6* is displayed. Not illuminated areas are simply blanked out. The bottom layer of the model at 1000 km depth is not shown, being very similar to the shallower one (950 km). See text for details.

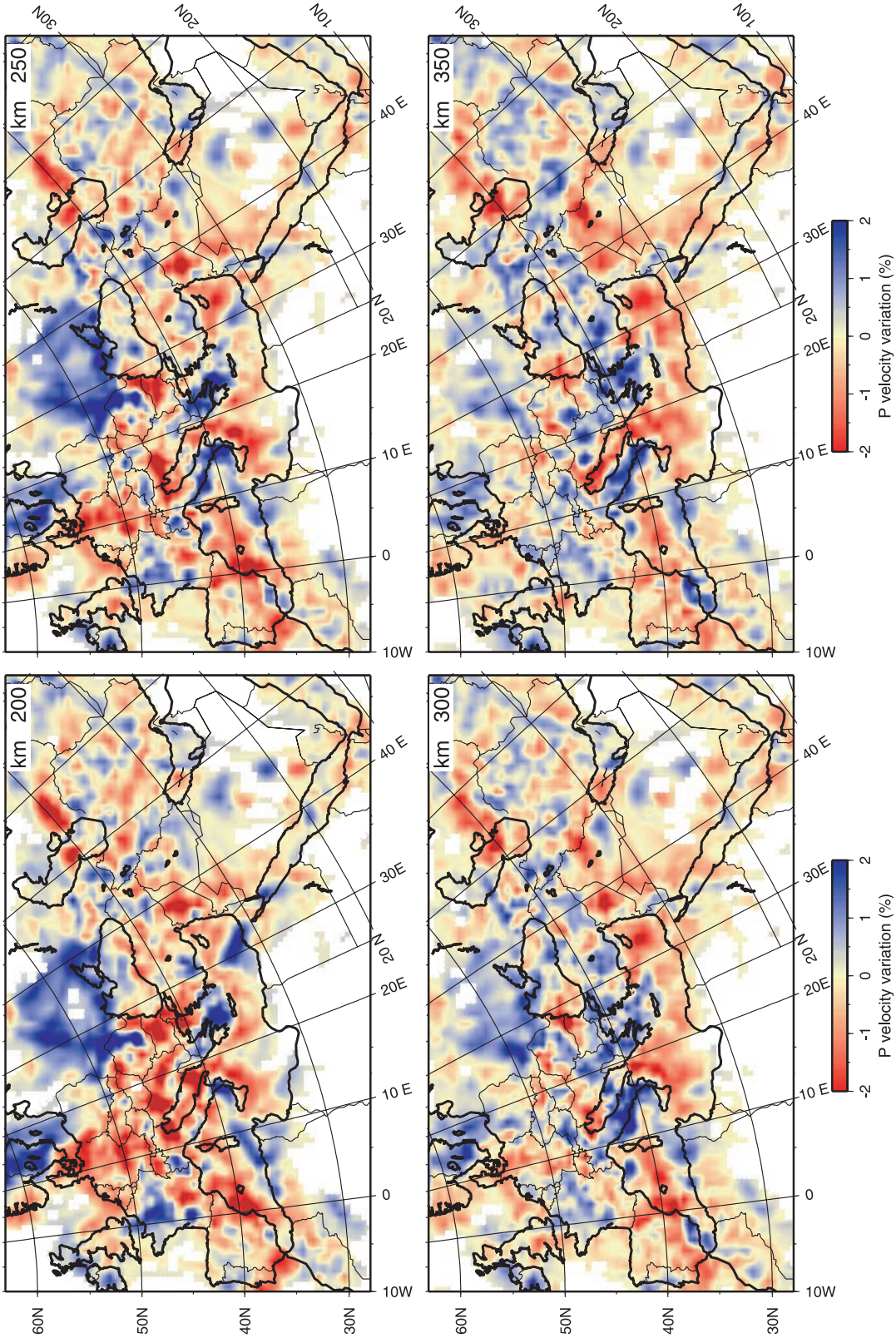

Figure 8. (continued)

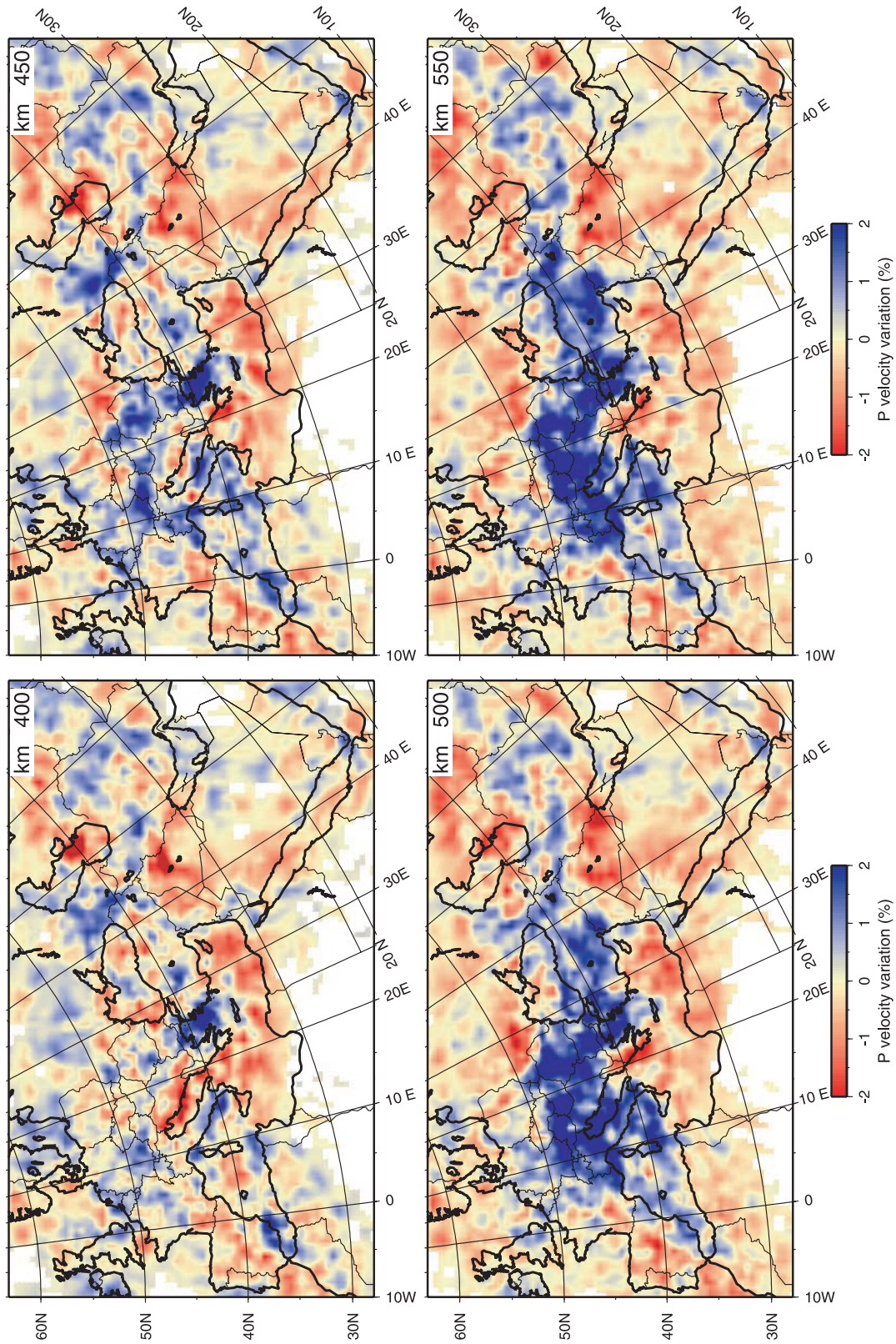

Figure 8. (continued)

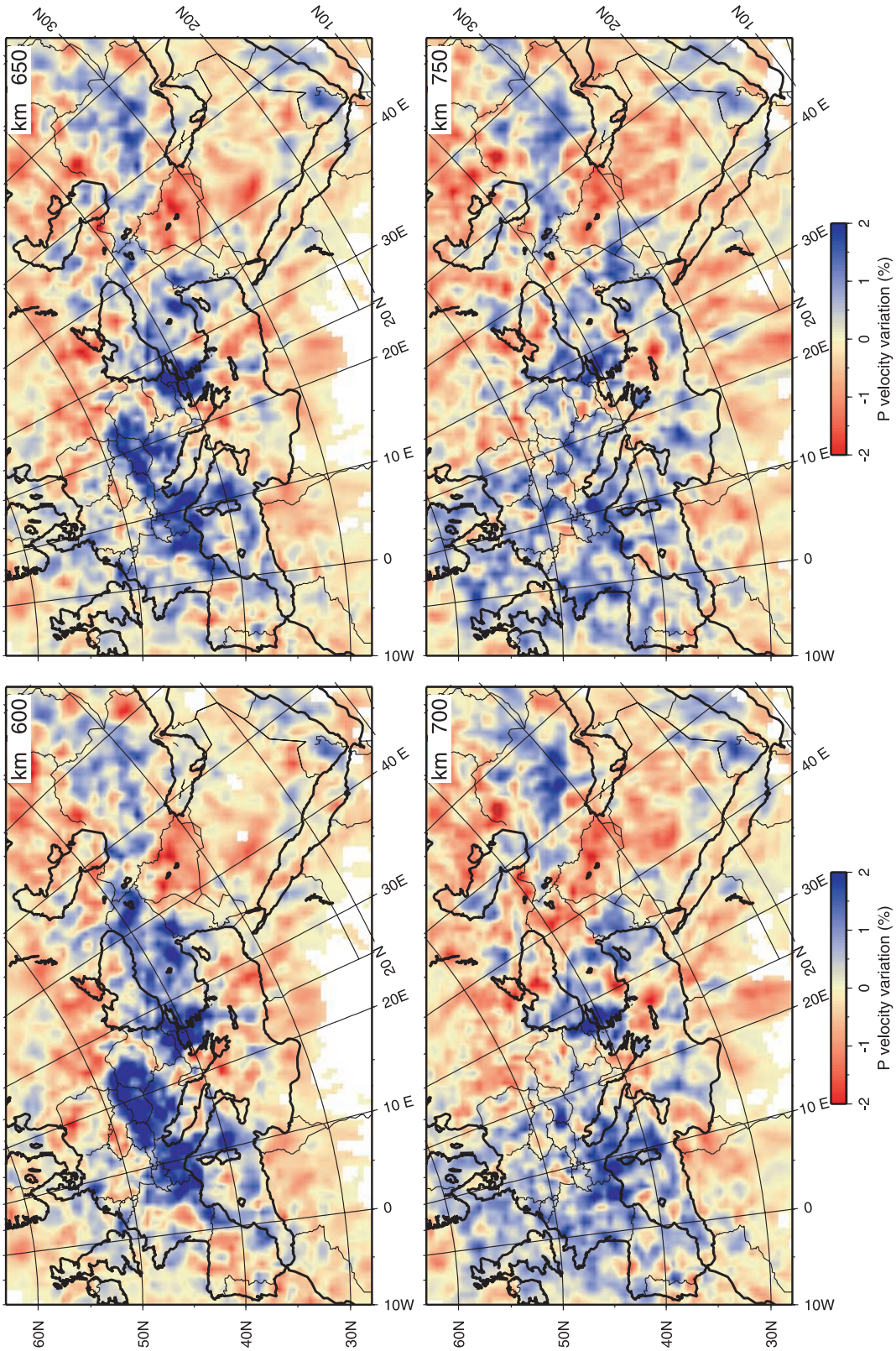

Figure 8. (continued)

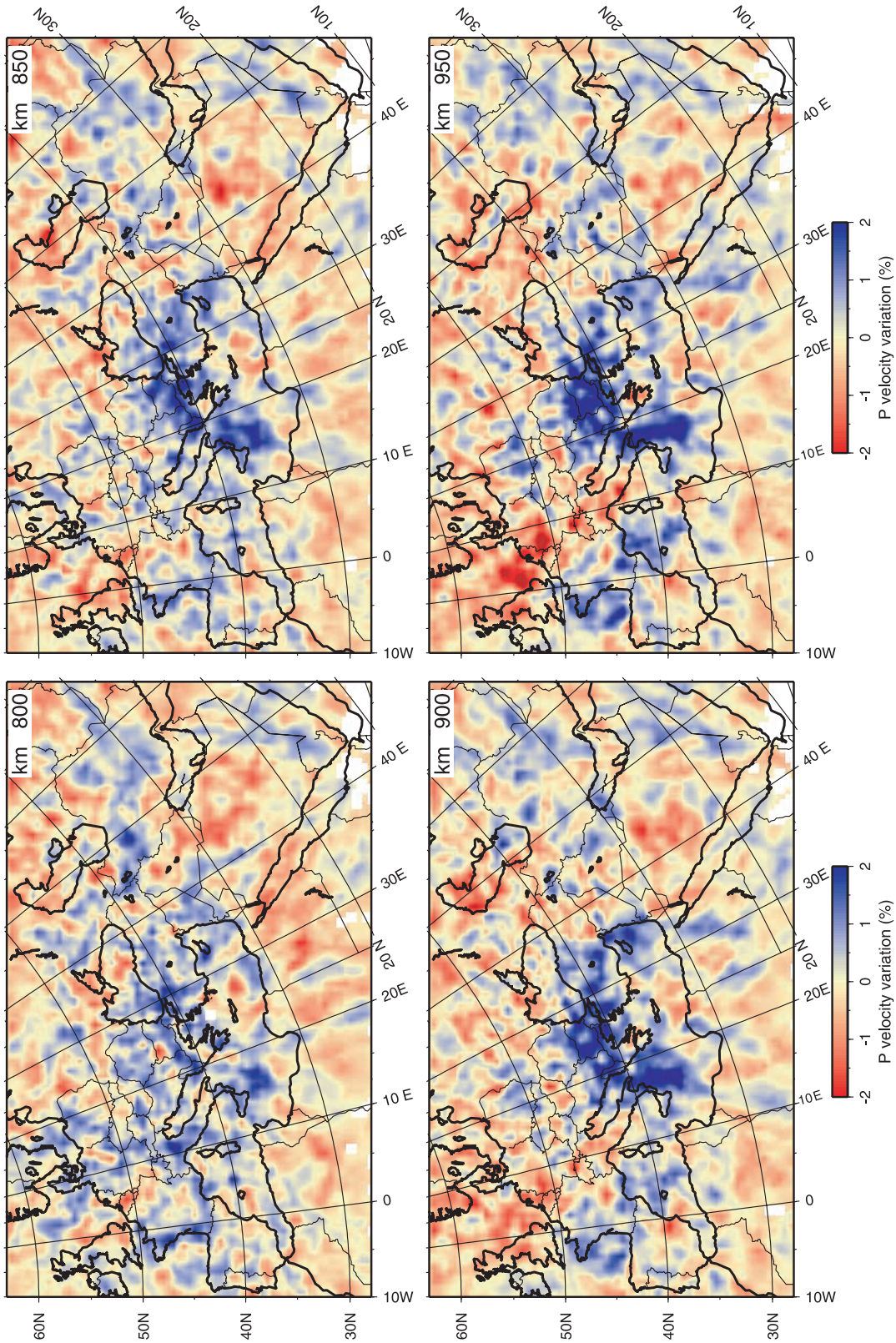

Figure 8. (continued)

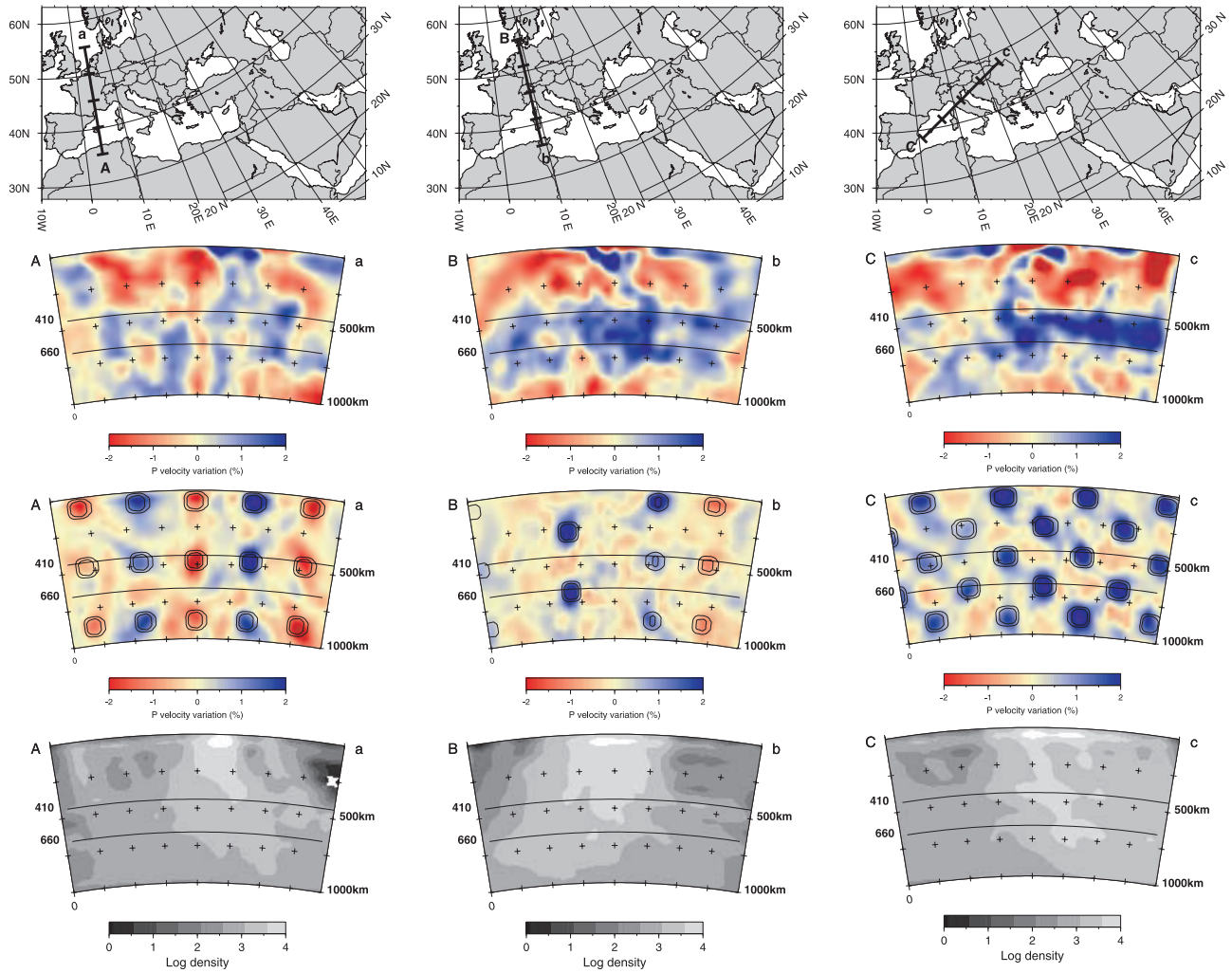

Figure 9. Cross sections through some of the main features of the velocity model. The top map illustrates the section location. Each cross section has the same length (approximately 20° along a great circle) and its vertical extent reaches the bottom of the model. Ticks along the line segment indicate the distance from the extremities by 5° intervals. Below the map, three panels are plotted: the top panel for the model, the central panel for the impulse recovery test results (contour levels of the input model at ±1% and ±3% are shown), and the bottom panel for the ray density distribution. Ticks at 5° intervals along the upper axis of each panel correspond to the locations along the section line segment plotted on the map. The 410 and 660 km discontinuities are indicated as a thin and thick lines, respectively. (Aa) Low velocity heterogeneity beneath the Massif Central (topmost 250 km). The synthetic test shows that the central portion of the section is well resolved, but some vertical leaking occurs and the narrow, conduit-like structure is probably not a robust feature. (Bb) Section running approximately along the European Geotraverse [*Blundell et al.*, 1992]. A fast feature deepens from the surface below the central Alps, its strongest portion reaching about 200 km depth. From ray sampling and the impulse recovery test, we expect a good resolution in the central portion of the section. Notice also the accumulation of fast material between 400 and 800 km. (Cc) Shallow fast anomaly below the northern Adriatic Sea possibly connected with the fast structure, below the northern Apennines. On the Tyrrhenian side, a wedge-shaped slow anomaly just above the slab merges with the lower amplitude western Mediterranean slow anomaly down to 400 km depth. (Dd) Strong slow anomaly beneath the central Apennines (0–250 km depth). To the east, the fast Adriatic lithosphere deepens below the Dinarides. (Ee) High velocity anomaly on the Ionian side of the Calabrian Arc connected to the fast structure steeply dipping below the arc into the mantle and bending horizontally in the transition zone. The synthetic test indicates that horizontal smearing may result in artifacts along this section at midmantle depths. (Ff) Fast material can be followed from the surface through the upper mantle, across the 670 km discontinuity and down to the bottom of the model in the Hellenic Trench. A large amplitude, well sampled, low anomaly wedge is found in correspondence of the Aegean Basin. Correlation between density of rays and shape of input anomalies indicates that smearing of these small anomalies likely occurs in the deeper part.

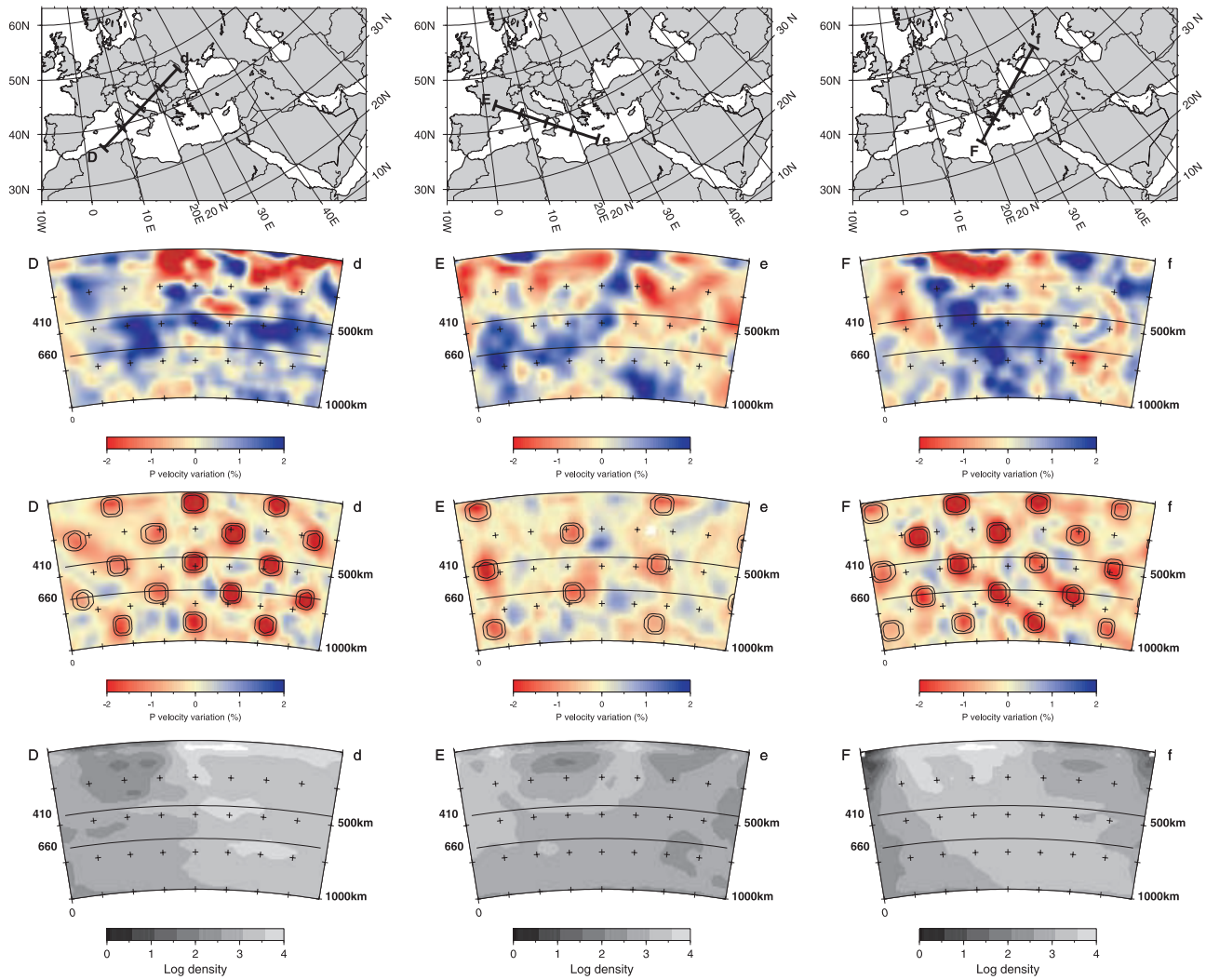

Figure 9. (continued)

scale models. *Seber et al.* [1996a] image a high velocity body beneath the Alboran Sea extending to the eastern Rif area as well, from subcrustal depths down to 350 km (bottom of their model). However, the limited vertical dimension of their model does not allow to evaluate the effective depth extent of the fast anomaly, which we show to enter into the transition zone. *Calvert et al.* [2000], though imaging fast anomalies also in the deep layers of their model (down to 670 km), discard the existence of a whole coherent body, favoring instead the hypothesis of two smaller pieces of delaminated lithospheric material.

[37] Pronounced low velocity anomalies are displayed by PM0.5 in the shallow layers below the Massif Central, Rhenish Massif and Bohemian Massif, coalescing into a broad anomaly in the 150–250 km depth range. The bulk of this low velocity perturbation resides in the shallowest 200–250 km and gradually attenuates in amplitude while approaching the transition zone. These heterogeneities in central Europe cover a wide region in correspondence of the ECRIS volcanic province, a belt of extensional thinning and rifting [*Wilson and Downes*, 1992; *Ziegler*, 1992]. Below the French Massif Central (cross section Aa, Figure 9) the main low velocity body extends from the surface down to 250 km depth, showing very good agreement with the local high-resolution teleseismic model of *Granet et al.* [1995]. In the Eifel region (Rhenish Massif), instead, *Ritter et al.* [2001] find evidence of low velocities down to at least 400 km, deeper than in PM0.5. Some studies, combining tomographic images with signatures from isotope geochemistry of mafic volcanic rocks of this province, led to reconsider active mantle upwellings as sources of rifting and volcanism [*Granet et al.*, 1995; *Hoernle et al.*, 1995; *Goes et al.*, 1999], as suggested in previous literature [*Duncan et al.*, 1972; *Froidevaux et al.*, 1974]. However, the detection of a possible direct, lower mantle, origin of such upwellings by means of seismic studies is hampered, on one side, by the insufficient resolution at depth of larger-scale tomographic models, and, on the other hand, by the limited depth extent of higher-resolution local studies. Although below the Massif Central and the Rhine region well-resolved slow anomalies are also present at the base of PM0.5 (see map views at 700–1000 km), the velocity pattern is rather weak and heterogeneous in the transition zone below the ECRIS. Robust evidence for a direct lower mantle feeding (i.e., a conduit-like feature) of the shallow low velocity anomalies is missing. Where a weak stem-like

feature is imaged, such as below the Massif Central, it is at the very limit of our resolution.

[38] The whole Alpine chain is underlain by high velocities in a continuous belt down to 150 km. In the western Alps a sharp boundary is detected between slow velocity along the northwestern border of the chain, and a strong fast anomaly to the east. In the deeper layers (200–250 km) anomalies are weaker and the western and eastern Alps appear to be horizontally disconnected from each other and from the fast anomaly below the Dinaric chain. A detailed mapping of these shallow anomalies is absent in the results by *Spakman et al.* [1993], likely due to the coarser parameterization of their model. Fast velocity features rejoin at depth (starting at about 300 km) and connect to the whole Alpine fast belt. In the western and central Alps the signature of the fast anomaly is particularly pronounced from 50 down to 300–350 km (cross section Bb, Figure 9) and is unanimously interpreted as the "root" of the Alps, the Eurasian lithosphere southwardly subducted below the Adriatic promontory [*Kissling and Spakman*, 1996]. Across the eastern Alps instead we do not find evidence of such a clear pattern of subduction: the high velocity features of the Eurasian and Adriatic lithospheres both seem to be only weakly connected with the deep seated (100–400 km) body. The difference between the deep structure of western and eastern Alps [*Panza and Mueller*, 1979; *Babuska et al.*, 1990] is here imaged with better detail than in studies based on teleseismic data alone [*Amato et al.*, 1993; *Solarino et al.*, 1996; *Lucente et al.*, 1999]. Moreover, according to our tests, imaging capabilities of PM0.5 should not be crucially different between the western and eastern arcs.

[39] Along the Apenninic chain two major velocity features are recognized: while in the northern part a high velocity structure is particularly evident in the layers between 100 and 200 km (cross section Cc, Figure 9), in the southern part a slow anomaly is instead found at these depths (cross section Dd, Figure 9). To the south, right below the Calabrian Arc, a fast velocity structure can be seen again in the shallow layers (100–200 km depth). Cross section Ee (Figure 9) shows the vertical extent and continuity of this fast feature, lying horizontal in the Ionian domain, steeply dipping to the NW in the mantle and then bending to almost horizontal in the transition zone. At 250 km and deeper, northern and southern Apennines join into the single, fast anomaly belt running southward with continuity through the Calabrian and North African margin, and northward through the Alps and Carpathians. A pronounced shallow slow anomaly is detected on the Tyrrhenian side, in correspondence of the back arc region, interpreted as the evidence of an asthenospheric wedge [*Mele et al.*, 1998; *Hearn*, 1999]. While in the Calabrian portion the subducted lithosphere is imaged with continuity by the vast majority of tomographic models [*Amato et al.*, 1993; *Spakman et al.*, 1993; *Selvaggi and Chiarabba*, 1995; *Piromallo and Morelli*, 1997; *Lucente et al.*, 1999], vertical continuity of the slab in its shallow portion below the Apenninic belt is instead a point of discrepancy. Since some models [*Spakman*, 1991; *Spakman et al.*, 1993] show no apparent connection between the Adriatic plate and the subducted lithosphere under the Apennines, *Wortel and Spakman* [1992] proposed a model of lateral migration of slab detachment from northwestern Italy to the Calabrian Arc. However, we note that the same northern Apenninic cross section shows enhanced vertical continuity in model BSE [*Bijwaard et al.*, 1998] with respect to EUR89B [*Spakman et al.*, 1993] (see the study of *Carminati et al.* [1998, Figure 7c]), displaying a velocity structure much closer to the one retrieved in both PM97P and PM0.5. Also teleseimic studies do not reveal any significant gap in the subducted lithosphere below the central Apennines [*Amato et al.*, 1993; *Lucente et al.*, 1999]; however, in these models the signal of a shallow positive anomaly could be easily obscured by smearing along teleseismic ray paths of a deeper, consistent, fast anomaly.

[40] The entire Carpathian chain is underlain by slow anomalies at shallow depths of PM0.5 (50 km), in sharp contrast with the fast velocities of the cratonic east European platform. In the eastern Carpathians, below the Vrancea zone, a weak fast velocity anomaly is present at 100 km depth, becoming more pronounced in the following layer (150 km). As depth increases, positive velocities tend to dominate below the whole chain, as a hook-shaped anomaly in map views (200–250 km). Regional tomographic studies have focused their attention on the Vrancea zone, also imaging a fast body in correspondence of the intermediate-depth earthquake foci, interpreted as a piece of subducted lithosphere [*Oncescu et al.*, 1984; *Fan et al.*, 1998; *Wenzel et al.*, 1998]. However, lack of resolution does not allow to establish the vertical extent of the high velocity body in these models. Only larger-scale studies like PM0.5 allow to detect anomalies at depth larger than the seismically active part of the slab, and they suggest that the deep portion of the slab may easily extend down to 300 km. Images of the shallow velocity structure retrieved by different models of the Vrancea zone led to different interpretations of the origin and nature of the fast velocity anomaly: the remnant of a slab of oceanic lithosphere now detached from the surface [*Wortel and Spakman*, 1992; *Wenzel et al.*, 1998], or instead a small fragment of oceanic lithosphere still attached to a larger piece of continental lithosphere [*Fan et al.*, 1998]. *Wortel and Spakman* [2000] favor the view of a continuous slab down to 350 km. Our model does not show, instead, any robust continuity to the surface of the Vrancea fast anomaly. This is an interesting open question, which needs further attention.

[41] The Hellenic Arc is marked by positive anomalies, approximately following its changes in strike. In the shallow layers these heterogeneities show continuity to the NW with the fast velocities below the Dinaric chain. The high velocity anomaly can be easily followed from shallow lithospheric depths across the transition zone and below, to the bottom of the model (cross section Ff, Figure 9), especially in correspondence of the W-SW portion of the Hellenic Arc. The high velocity anomaly sinks at an angle of about 45° in the upper mantle, while its shallower portion appears to dip on a less steep plane. As depth increases, fast material along the arc converges towards the northern Aegean (map views) and appears to be only partly deflected in correspondence of the 660 km discontinuity (cross section Ff, Figure 9). At 50 km depth the whole Aegean Sea in the back arc setting is dominated by a wide, pronounced, slow anomaly, which shifts northward and attenuates at increasing depths, down to about 250 km. The Cyprus Arc is well delimited at shallow depths by the cold Levantine lithosphere. A small fast velocity anomaly, NW of Cyprus, joins across the Antalya Basin, in corre-

spondence of the trench's cusp, with the more pronounced anomaly below Turkey, which can be followed down to the transition zone. The fast anomaly below the Hellenic Arc, interpreted as African lithosphere subducted beneath the Aegean, is imaged by both regional studies [*Spakman et al.*, 1988; *Granet and Trampert*, 1989; *Ligdas and Main*, 1991; *Spakman*, 1991; *Piromallo and Morelli*, 1997; *Tiberi et al.*, 2000] and larger-scale models, which show that it reaches the lower mantle [*Spakman et al.*, 1993; *van der Hilst et al.*, 1997; *Bijwaard et al.*, 1998; this work]. Since the observation by *Spakman et al.* [1988] of a discontinuity in the subducted slab at a depth of 100–250 km, as a horizontal tear in the north and western portions of the arc, the hypothesis of detachment of the deeper part of the slab from the surface has been put forward [*Wortel and Spakman*, 1992, 2000]. However, from the map views of our model we see a possible interruption in the fast anomaly only at 100–150 km in a very limited area below mainland Greece and it is hard to assess its effective robustness. Moreover, high-resolution local studies of the crust and topmost mantle [*Papazachos et al.*, 1995; *Papazachos and Nolet*, 1997] do not detect any gap at all in the slab at these shallow depths.

6. Discussion

[42] The presence of seismically fast material in the transition zone and below raises the question about the nature of such heterogeneities, and on the style of present-day mantle convection in the Alpine-Mediterranean region. Lateral variations in seismic velocities reported at all depths in the mantle from tomographic observations have been usually interpreted in terms of thermal structure related to convection. Though both temperature and composition may influence wave speeds, most of the 3-D mantle velocity variation can probably be attributed to changes in temperature [e.g., *Ranalli*, 1996], the effect of mantle composition contributing only less than 1% [*Sobolev et al.*, 1997; *Goes et al.*, 2000]. Interpreting the deep high velocity anomalies as mainly related to "cold" material, the snapshot of the present-day large-scale features given by tomographic pictures can provide important information both in the framework of global geodynamics and in the discussion of specific evolutionary scenarios for the Mediterranean. The pattern of large-scale anomalies revealed by PM0.5 suggests that two different convection stages presently coexist in very close regions. The mantle dynamics of western central Europe are dominated by layering, with blockage of subducted slabs at the 660 km discontinuity and consequent accumulation of seismically fast material in the transition zone [*Piromallo et al.*, 2001]. On the contrary, in the eastern Mediterranean a substantial amount of fast velocity material appears to sink into the lower mantle (even deeper than 1000 km, according to *van der Hilst et al.* [1997]), suggesting that the flow of the cold downwelling here is not barred by the 660 km discontinuity. The extent of mantle layering under Europe has been estimated through wavelet analysis of the seismic anomalies of PM0.5 by focussing on the different length scales in the correlation function [*Piromallo et al.*, 2001]. Between the depths of 500 and 600 km under western central Europe this correlation analysis shows that a strong correlation for long length scales, of around 400 km, exists over a wide area of about 2000 × 4000 km, while weaker correlation characterizes shorter length scales (150 km). On the other hand, between layers at depths of 400 and 600 km the correlation deteriorates on the long length scales and becomes even worse at the short length scales. These results suggest that the thickness of the recumbent fast (cold) material in the transition zone is between 100 and 150 km. Moreover, the correlation between the layer at 600 km and those at larger depth shows a clear shift of the strong coherence to the eastern Mediterranean, where indeed a substantial amount of fast velocity material appears to sink into the lower mantle [see also *van der Hilst et al.*, 1997]. A possible explanation of this scenario is that in the eastern Mediterranean, the longer duration of subduction (active from the Cretaceous or possibly the Jurassic rather than from the Tertiary) and the different motion of the upper plate–trench system with respect to the western Mediterranean, favored the sinking in the mantle of a large amount of lithospheric material and its piling up at the upper–lower mantle boundary. Accumulation would overcome the effects of the viscosity jump and of the endothermic phase transition, causing the eventual flush of material to the lower mantle. The past subduction history which possibly led to the present-day scenario and the implications for the style of mantle convection are inspected in detail elsewhere [*Faccenna et al.*, 2003], tying together geological data, paleotectonic reconstructions, plate motion and tomographic data.

[43] In some tomographic models [*Spakman*, 1990; *Spakman et al.*, 1993] the absence of continuity in the images of structures identified as subducted slabs has been interpreted by the authors in the common frame of a near surface lithospheric detachment process, characterizing and influencing the tectonic evolution of the Euro-Mediterranean region [*Wortel and Spakman*, 1992]. However, in many cases the interruption in the distribution of the high velocity anomalies does not appear to be a consistent feature among different studies. More recent, better resolved, models seem to exhibit more vertical continuity of fast structures than older models. Many causes may affect the continuity of slab images: inhomogeneous sampling, data density, reference model, parameterization, damping, ray tracing technique. As shown by sensitivity analyses vertical gaps in tomographic images of slabs as large as 50–60 km or less cannot be quantitatively resolved by regional-scale tomographic models [*Spakman*, 1990; *Spakman et al.*, 1993; *Piromallo and Morelli*, 1997; *Bijwaard et al.*, 1998; *Lucente et al.*, 1999; this work]. Though of course the existence of small features cannot be ruled out, too detailed interpretation of tomographic models, which may go beyond the resolution, should be avoided. Sticking to robust features, model PM0.5 shows a strong, robust, difference between the northern and southern Apennines in the top 200 km. While below the northern portion of the chain we find a fast anomaly at all depths, below the southern part a pronounced, wide and well-resolved slow anomaly is present. Along the Dinaric-Hellenic chain, instead, a pronounced fast velocity anomaly can be followed at all depths in the central southern portion, while a slow anomaly dominates the northernmost part down to the top of the transition zone. Therefore, the hypothesis of lateral migration of slab detachment, proposed by *Wortel and Spakman* [1992, 2000] as a unifying process taking place on

both sides of the Adriatic plate, is not supported by our results, which depict instead a more complex scenery deserving further investigation.

7. Concluding Remarks

[44] Mantle structure in the Euro-Mediterranean region has been studied at different levels of detail by many authors for more than two decades. This study was motivated by the goal of further enhancing the detail of the tomographic image, in a wide-scale model. While confirming the general view of the lithosphere and mantle structure of the region, we also present important differences that may provide new insight into active geodynamic processes.

[45] The main 3-D large-scale and small-scale features detected by our model PM0.5 are generally in fair correspondence with those obtained by other *P* wave studies with similar or slightly lower resolution. Fair agreement is found with model EUR89B [*Spakman et al.*, 1993], spanning approximately the same area as PM0.5. However, the coarser parameterization of EUR89B and the reference model adopted are responsible for some apparent differences in the detailed structure. *Spakman et al.* [1993] used a background reference model with a low velocity layer in the 120–250 km depth range and a small negative velocity gradient. Fast velocity anomalies at sublithospheric depths are often more discontinuous in EUR89B than in studies based on background models with a positive velocity gradient throughout the upper mantle. A low velocity layer is not present in modern global reference models [*Kennett and Engdahl*, 1991; *Morelli and Dziewonski*, 1993; *Kennett et al.*, 1995], nor we find evidence for it in the average velocity profile for our region. In fact, the average radial velocity perturbation (Figure 6) is so small that the new profile does not differ appreciably from the reference model. Enhanced vertical continuity is shared, for instance, by BSE [*Bijwaard et al.*, 1998] and PM0.5.

[46] We have shown that there are good similarities between our model and BSE [*Bijwaard et al.*, 1998], result of a global inversion with variable resolution. A main difference between models BSE and PM0.5, on one side, and the class of previous models, on the other side, consists of explicit allowance, in newer approaches, of heterogeneous structure in the whole mantle. BSE is obtained through actual inversion for global P velocity structure; whereas in PM0.5 we instead focus on inversion in a specific geographic region, but we minimize the effect of global Earth structure outside the study volume (be it heterogeneity or anisotropy or a systematic station bias) through the use of averaged path corrections. Both approaches have advantages and disadvantages, and can be seen as aimed at partly differing goals. A global-scale inversion represents the conceptually most complete approach, and today it can be pushed to quite high resolution by modern availability of computing power, but it has to face an increased complexity and to tackle with potential sources of disturbance such as the extremely irregular data coverage of the globe. Our approach, although of course limited to the study of a specific geographical region with good data coverage, has the advantage of extreme computational simplicity and bypasses sources of instabilities, at the cost of a less faithful, ad hoc, description of external Earth structure. BSE differs from PM0.5 also for many other choices, among which the most important are the EHB data set [*Engdahl et al.*, 1998], the parameterization in irregular blocks, the depth extent of the model (2900 km), the nominal resolution in the upper mantle (up to 0.6°), the reference model adopted (*ak135*), the joint inversion for velocity, relocation vectors and station corrections, the explicit regularization applied (depth and cell volume dependent second derivative damping). With so many procedural differences, agreement of the results has good significance.

[47] The linearized approach of our tomographic method is another simplification we adopt. In presence of sharp velocity gradients as in the shallowest portion of the Earth, data cannot be considered insensitive to approximations of ray geometry and 3-D ray tracing may be required to obtain more accurate images. The nonlinear effect is proved to be particularly significant for strongly heterogeneous models, producing an overall focusing of structures: a slight change in anomaly patterns, a small increase in variance reduction and model amplitudes, and a baseline shift towards low velocities [*Papazachos and Nolet*, 1997; *Bijwaard and Spakman*, 2000]. However, resulting images do not differ conceptually from the outcome of a linearized inversion with 1-D ray tracing [*Bijwaard and Spakman*, 2000]. The use of regional phases, which propagate in very heterogeneous structures, where velocity perturbations may be stronger than a few percent, implies a probable smoothing effect, but no important mistakes, induced by the 1-D algorithm. The interpretation of regional seismic phases is problematic also because their onset is often difficult to pick due, for example, to triplication. Alternative approaches, avoiding this difficulty, involve fitting entire waveforms or surface wave phase and group velocity observation, but cannot reach the spatial resolution attained by travel time tomography.

[48] Amplitudes of velocity anomalies are not very well constrained and sensitivity test results suggest that RMS amplitudes of the reconstructed model may be as small as 60% of the input pattern. Moreover, they decrease as ray sampling decreases, an effect inherent to the inversion algorithm. The retrieved perturbation may underestimate the actual values because of the effect of regularization (damping) of the inversion, trade-off with earthquake location (the hypocenter parameters during the preliminary location can in principle have absorbed substantial signal) and the neglect of ray-bending effects, which provides a defocusing effect. The inability to assess with confidence the amplitudes of velocity anomalies is one of the serious limits of tomographic imaging, still hindering more quantitative interpretation of tomographic results.

[49] **Acknowledgments.** We appreciate the critical review by Rob van der Hilst. This paper benefited from comments by Michel Granet and Lapo Boschi, which greatly improved the manuscript. We acknowledge fruitful discussions with Wim Spakman, Claudio Faccenna, and Dave Yuen. We thank Enzo Boschi for his continuing encouragement and support. All figures were created using Generic Mapping Tools (GMT) [*Wessel and Smith*, 1991].

References

Amato, A., B. Alessandrini, and G. B. Cimini, Teleseismic tomography of Italy, in *Seismic Tomography: Theory and Practice*, edited by H. M. Iyer and K. Hirahara, pp. 361–396, Chapman and Hall, New York, 1993.

Babuska, V., J. Plomerova, and M. Granet, The deep lithosphere in the Alps: A model inferred from P residuals, *Tectonophysics*, *176*, 137–165, 1990.

Bijwaard, H., and W. Spakman, Non-linear global P-wave tomography by iterated linearized inversion, *Geophys. J. Int.*, *141*, 71–82, 2000.

Bijwaard, H., W. Spakman, and R. Engdahl, Closing the gap between regional and global travel time tomography, *J. Geophys. Res.*, *103*, 30,055–30,078, 1998.

Blanco, M. J., and W. Spakman, The P-wave velocity structure of the mantle below the Iberian Peninsula: Evidence for subducted lithosphere below southern Spain, *Tectonophysics*, *221*, 13–34, 1993.

Blundell, D., R. Freeman, and S. Mueller, A continent revealed, in *A Continent Revealed*, edited by D. Blundell et al., p. 275, Cambridge Univ. Press, New York, 1992.

Buland, R., and C. H. Chapman, The computation of seismic travel times, *Bull. Seismol. Soc. Am.*, *73*, 1271–1302, 1983.

Calcagnile, G., and G. F. Panza, Crustal and upper mantle structure of the Mediterranean area derived from surface-wave data, *Phys. Earth Planet. Inter.*, *60*, 163–168, 1990.

Calvert, A., E. Sandvol, D. Seber, M. Barazangi, S. Roecker, T. Mourabit, F. Vidal, G. Alguacil, and N. Jabour, Geodynamic evolution of the lithosphere and upper mantle beneath the Alboran region of the western Mediterranean: Constraints from travel time tomography, *J. Geophys. Res.*, *105*, 10,871–10,898, 2000.

Carminati, E., M. J. R. Wortel, W. Spakman, and R. Sabadini, The role of slab detachment processes in the opening of the western-central Mediterranean basins: Some geological and geophysical evidence, *Earth Planet. Sci. Lett.*, *160*, 651–665, 1998.

Curtis, A., J. Trampert, R. Snieder, and B. Dost, Eurasian fundamental mode surface wave phase velocities and their relationship with tectonic structures, *J. Geophys. Res.*, *103*, 26,919–26,947, 1998.

Dercourt, J., et al., Geological evolution of the from the Atlantic to the Pamirs since the Lias, *Tectonophysics*, *123*, 241–315, 1986.

Dewey, J. F., M. L. Helman, E. Turco, D. H. Hutton, and S. D. Knott, Kinematics of the western Mediterranean, in *Alpine Tectonics, Geol. Soc. Spec. Publ.*, edited by M. P. Coward et al., *45*, 265–283, 1989.

Duncan, R. A., N. Petersen, and R. Hargraves, Mantle plumes, movement of the European Plate, and polar wandering, *Nature*, *239*, 82–86, 1972.

Dziewonski, A. M., and D. L. Anderson, Travel times and station corrections for P waves at teleseismic distances, *J. Geophys. Res.*, *88*, 3295–3314, 1983.

Dziewonski, A. M., and F. Gilbert, The effect of small aspherical perturbations on travel times and a re-examination of the corrections for ellipticity, *Geophys. J. R. Astron. Soc.*, *44*, 7–16, 1976.

Engdahl, R., R. van der Hilst, and R. Buland, Global teleseismic earthquake relocation with improved travel times and procedures for depth determination, *Bull. Seismol. Soc. Am.*, *88*, 722–743, 1998.

Faccenna, C., L. Jolivet, C. Piromallo, and A. Morelli, Subduction and the depth of convection in the Mediterranean mantle, *J. Geophys. Res.*, *108*, doi:10.1029/2001JB001690, in press, 2003.

Fan, G., T. C. Wallace, and D. Zhao, Tomographic imaging of deep velocity structure beneath the eastern and southern Carpathians, Romania: Implications for continental collision, *J. Geophys. Res.*, *103*, 2705–2723, 1998.

Froidevaux, C., R. Brousse, and H. Bellon, Hot spot in France?, *Nature*, *248*, 749–751, 1974.

Fukao, Y., M. Obayashi, and H. Inoue, Subducting slabs stagnant in the mantle transition zone, *J. Geophys. Res.*, *97*, 4822–4909, 1992.

Fukao, Y., S. Widiyantoro, and M. Obayashi, Stagnant slabs in the upper and lower mantle transition region, *Rev. Geophys.*, *39*, 291–323, 2001.

Glahn, A., and M. Granet, Southern Rhine Graben: Small-wavelength tomographic study and implications for the dynamic evolution of the graben, *Geophys. J. Int.*, *113*, 399–418, 1993.

Goes, S., W. Spakman, and H. Bijwaard, A lower mantle source for central European volcanism, *Science*, *286*, 1928–1931, 1999.

Goes, S., R. Govers, and P. Vacher, Shallow mantle temperatures under Europe from P and S wave tomography, *J. Geophys. Res.*, *105*, 11,153–11,169, 2000.

Grand, S., A possible station bias in travel time measurements reported to ISC, *Geophys. Res. Lett.*, *17*, 17–20, 1990.

Grand, S. P., R. D. van der Hilst, and S. Widiyantoro, High resolution global tomography: A snapshot of convection in the Earth, *GSA Today*, *7*, 1–7, 1997.

Granet, M., and J. Trampert, Large-scale P velocity structures in the Euro-Mediterranean area, *Geophys. J. Int.*, *99*, 583–594, 1989.

Granet, M., M. Wilson, and U. Achauer, Imaging a mantle plume beneath the Massif Central (France), *Earth Planet. Sci. Lett.*, *136*, 281–296, 1995.

Gudmundsson, O., J. H. Davies, and R. W. Clayton, Stochastic analysis of global traveltime data: Mantle heterogeneity and random errors in the ISC data, *Geophys. J. Int.*, *102*, 25–43, 1990.

Hager, B. H., and R. W. Clayton, Constraints on the structure of mantle convection using seismic observations, flow models, and the geoid, in *Mantle Convection*, edited by W. R. Peltier, pp. 657–763, Gordon and Breach, Newark, N. J., 1989.

Hearn, T. M., Uppermost mantle velocities and anisotropy beneath Europe, *J. Geophys. Res.*, *104*, 15,123–15,139, 1999.

Hoernle, K., Y.-S. Zhang, and D. Graham, Seismic and geochemical evidence for large-scale mantle upwelling beneath the eastern Atlantic and western and central Europe, *Nature*, *374*, 34–39, 1995.

Horvath, F., and H. Berckhemer, Mediterranean back-arc basins, in *Alpine–Mediterranean Geodynamics, Geodyn. Ser.*, vol. 7, edited by H. Berkhemer and K. J. Hsü, pp. 141–174, AGU, Washington, D. C., 1982.

Hovland, J., D. Gubbins, and E. S. Husebye, Upper mantle heterogeneities beneath Central Europe, *Geophys. J. R. Astron. Soc.*, *66*, 261–284, 1981.

International Seismological Centre, Bulletin Disks 1–6, Int. Seismol. Cent., Thatcham, UK, 1997.

Jeffreys, H., An alternative to the rejection of observations, *Proc. R. Soc. London, Ser. A*, *187*, 78–87, 1932.

Jeffreys, H., and K. E. Bullen, *Seismological Tables*, Br. Assoc. for the Adv. of Sci., London, 1940.

Kárason, H., and R. D. van der Hilst, Tomographic imaging of the lowermost mantle with differential times of refracted and diffracted core phases (PKP, Pdiff), *J. Geophys. Res.*, *106*, 6569–6588, 2001.

Kennett, B. L. N., and E. R. Engdahl, Traveltimes for global earthquake location and phase identification, *Geophys. J. Int.*, *105*, 429–465, 1991.

Kennett, B. L. N., E. R. Engdahl, and R. Buland, Constraints on seismic velocities in the Earth from traveltimes, *Geophys. J. Int.*, *122*, 108–124, 1995.

Kissling, E., and W. Spakman, Interpretation of tomographic images of uppermost mantle structure: Examples from the western and central Alps, *J. Geodyn.*, *21*, 97–111, 1996.

Lévêque, J.-J., L. Rivera, and G. Wittlinger, On the use of checker-board test to assess the resolution of tomographic inversions, *Geophys. J. Int.*, *115*, 313–318, 1993.

Ligdas, C. N., and I. G. Main, On the resolving power of tomographic images in the Aegean area, *Geophys. J. Int.*, *107*, 197–203, 1991.

Lucente, F. P., C. Chiarabba, G. B. Cimini, and D. Giardini, Tomographic constraints on the geodynamic evolution of the Italian region, *J. Geophys. Res.*, *104*, 20,307–20,327, 1999.

Malinverno, A., and W. B. F. Ryan, Extension in the Tyrrhenian sea and shortening in the Apennines as result of arc migration driven by sinking of the lithosphere, *Tectonics*, *5*, 227–245, 1986.

Marquering, H., and R. Snieder, Shear-wave velocity structure beneath Europe, the northeastern Atlantic and western Asia from waveform inversions including surface-wave mode coupling, *Geophys. J. Int.*, *127*, 283–304, 1996.

Mele, G., A. Rovelli, D. Seber, T. M. Hearn, and M. Barazangi, Compressional velocity structure and anisotropy in the uppermost mantle beneath Italy and surrounding regions, *J. Geophys. Res.*, *103*, 12,529–12,543, 1998.

Morelli, A., and A. Dziewonski, Joint determination of lateral heterogeneity and earthquake location, in *Glacial Isostasy, Sea-Level and Mantle Rheology*, edited by R. Sabadini et al., pp. 515–534, Kluwer Acad., Norwell, Mass., 1991.

Morelli, A., and A. Dziewonski, Body wave traveltimes and a spherically symmetric P- and S-wave velocity model, *Geophys. J. Int.*, *112*, 178–194, 1993.

Nolet, G., Seismic wave propagation and seismic tomography, in *Seismic Tomography*, edited by G. Nolet, pp. 1–23, D. Reidel, Norwell, Mass., 1987.

Nolet, G., A general view on the seismic inverse problem, in *Seismic Modelling of the Earth Structure*, edited by E. Boschi et al., pp. 1–27, Ed. Compositori, Bologna, Italy, 1996.

Nolet, G., Interpreting seismic waveforms: Forward and inverse problems for heterogeneous media, in *Problems in Geophysics for the Next Millennium*, edited by E. Boschi et al., pp. 373–401, Ed. Compositori, Bologna, Italy, 2000.

Oncescu, M. C., V. Burlacu, M. Angel, and V. Smalbergher, Three-dimensional P-wave velocity image under the Carpathian arc, *Tectonophysics*, *106*, 305–319, 1984.

Paige, C. C., and M. A. Saunders, LSQR: An algorithm for sparse linear equations and sparse least squares, *ACM Trans. Math. Software*, *8*, 43–71, 1982.

Panza, G. F., and S. Mueller, The plate boundary between Eurasia and Africa in the Alpine Area, *Mem. Sci. Geol.*, *33*, 43–50, 1979.

Panza, G. F., S. Mueller, and G. Calcagnile, The gross features of the lithosphere–asthenosphere system in Europe from seismic surface waves and body waves, *Pure Appl. Geophys.*, *118*, 1209–1213, 1980.

Papazachos, C., and G. Nolet, P and S deep velocity structure of the Hellenic area obtained by robust nonlinear inversion of travel times, *J. Geophys. Res.*, *102*, 8349–8367, 1997.

Papazachos, C. B., P. M. Hatzidimitriou, D. G. Panagiotopoulos, and G. N. Tsokas, Tomography of the crust and upper mantle in southeast Europe, *J. Geophys. Res.*, *100*, 12,405–12,442, 1995.

Piromallo, C., and A. Morelli, Imaging the Mediterranean upper mantle by P-wave travel time tomography, *Ann. Geofis.*, *XL*, 963–979, 1997.

Piromallo, C., and A. Morelli, P-wave propagation heterogeneity and earthquake location in the Mediterranean region, *Geophys. J. Int.*, *135*, 232–254, 1998.

Piromallo, C., and A. Morelli, Improving earthquake location: An alternative to three-dimensional structural models, *Pure Appl. Geophys.*, *158*, 319–347, 2001.

Piromallo, C., A. Vincent, D. Yuen, and A. Morelli, Dynamics of the transition zone under Europe inferred from wavelet cross-spectra of seismic tomography, *Phys. Earth Planet. Inter.*, *125*, 125–139, 2001.

Ranalli, G., Seismic tomography and mineral physics, in *Seismic Modelling of the Earth Structure*, edited by E. Boschi et al., pp. 443–459, Ed. Compositori, Bologna, Italy, 1996.

Ritter, J. R. R., M. Jordan, U. R. Christensen, and U. Achauer, A mantle plume below the Eifel volcanic fields, Germany, *Earth Planet. Sci. Lett.*, *186*, 7–14, 2001.

Ritzwoller, M. H., and A. L. Levshin, Eurasian surface wave tomography: Group velocities, *J. Geophys. Res.*, *103*, 4839–4878, 1998.

Robertson, G. S., and J. H. Woodhouse, Evidence for proportionality of P and S heterogeneity in the lower mantle, *Geophys. J. Int.*, *123*, 85–116, 1995.

Robertson, G. S., and J. H. Woodhouse, Comparison of P and S station corrections and their relationship to upper mantle structure, *J. Geophys. Res.*, *102*, 27,355–27,366, 1997.

Roecker, S. W., T. M. Sabitova, L. P. Vinnik, Y. A. Burmakov, M. I. Golvanov, R. Mamatkanova, and L. Munirova, Three-dimensional elastic-wave velocity structure of the western and central Tien Shan, *J. Geophys. Res.*, *98*, 15,779–15,795, 1993.

Rohm, A. H. E., J. Trampert, and R. K. Snieder, Bias in reported seismic arrival times deduced from the ISC, *Geophys. J. Int.*, *137*, 163–174, 1999.

Romanowicz, B. A., A study of large-scale lateral variations of P-velocity in the upper mantle beneath western Europe, *Geophys. J. R. Astron. Soc.*, *63*, 217–232, 1980.

Sambridge, M., and O. Gudmunsson, Tomography with irregular cells, *J. Geophys. Res.*, *103*, 773–781, 1998.

Seber, D., M. Barazangi, A. Ibenbrahim, and A. Demnati, Geophysical evidence for lithospheric delamination beneath the Alboran Sea and the Betic-Rif mountains, *Nature*, *379*, 785–790, 1996a.

Seber, D., M. Barazangi, B. A. Tadili, M. Ramdani, A. Ibenbrahim, and D. Ben Sari, Three-dimensional upper mantle structure beneath the intraplate Atlas and interplate Rif mountains of Morocco, *J. Geophys. Res.*, *101*, 3125–3138, 1996b.

Selvaggi, G., and C. Chiarabba, Seismicity and P-velocity image of the southern Tyrrhenian subduction zone, *Geophys. J. Int.*, *121*, 818–826, 1995.

Snieder, R., Large scale waveform inversions of surface waves for lateral heterogeneity, 2, Application to surface waves in Europe and the Mediterranean, *J. Geophys. Res.*, *93*, 12,067–12,080, 1988.

Sobolev, S. V., H. Zeyen, M. Granet, U. Achauer, C. Bauer, F. Werling, R. Altherr, and K. Fuchs, Upper mantle temperatures and lithosphere–asthenosphere system beneath the French Massif Central constrained by seismic, gravity, petrologic and thermal observations, *Tectonophysics*, *275*, 143–164, 1997.

Solarino, S., D. Spallarossa, S. Parolai, M. Cattaneo, and C. Eva, Litho-asthenospheric structures of northern Italy as inferred from teleseismic P-wave tomography, *Tectonophysics*, *260*, 271–289, 1996.

Spakman, W., Tomographic images of the upper mantle below central Europe and the Mediterranean, *Terra Nova*, *2*, 542–553, 1990.

Spakman, W., Delay-time tomography of the upper mantle below Europe, the Mediterranean and Asia Minor, *Geophys. J. Int.*, *107*, 309–332, 1991.

Spakman, W., and G. Nolet, Imaging algorithms, accuracy and resolution in delay time tomography, in *Mathematical Geophysics*, edited by N. J. Vlaar et al., pp. 155–187, D. Reidel, Norwell, Mass., 1988.

Spakman, W., M. J. R. Wortel, and N. J. Vlaar, The Hellenic subduction zone: A tomographic image and its geodynamic implications, *Geophys. Res. Lett.*, *15*, 60–63, 1988.

Spakman, W., S. van der Lee, and R. van der Hilst, Travel-time tomography of the European-Mediterranean mantle down to 1400 km, *Phys. Earth Planet. Inter.*, *79*, 3–74, 1993.

Tiberi, C., et al., Crustal and upper mantle structure beneath the Corinth rift (Greece) from a teleseismic tomography study, *J. Geophys. Res.*, *105*, 28,159–28,171, 2000.

van der Hilst, R. D., and E. R. Engdahl, On ISC pP and PP data and their use in delay time tomography of the Caribbean region, *Geophys. J. Int.*, *106*, 169–188, 1991.

van der Hilst, R. D., and H. Karason, Compositional heterogeneity in the bottom 1000 kilometers of Earth's mantle: Toward a hybrid convection model, *Science*, *283*, 1885–1888, 1999.

van der Hilst, R. D., E. R. Engdahl, and W. Spakman, Tomographic inversion of P and pP data for aspherical mantle structure below the northwest Pacific region, *Geophys. J. Int.*, *115*, 264–302, 1993.

van der Hilst, R. D., S. Widiyantoro, and R. Engdahl, Evidence for deep mantle circulation from global tomography, *Nature*, *386*, 578–584, 1997.

Wenzel, F., U. Achauer, D. Enescu, E. Kissling, R. Russo, V. Mocanu, and G. Musacchio, Detailed look at final stage of break-off is target of study in Romania, *Eos Trans. AGU*, *48*, 589–594, 1998.

Wessel, P., and W. H. F. Smith, Free software helps map and display data, *Eos Trans. AGU*, *72*, 441, 1991.

Widiyantoro, S., and R. D. van der Hilst, Structure and evolution of subducted lithosphere beneath the Sunda arc, Indonesia, *Science*, *271*, 1566–1570, 1996.

Wilson, M., and H. Downes, Mafic alkaline magmatism associated with the European Cenozoic rift system, *Tectonophysics*, *208*, 173–182, 1992.

Wortel, M. J. R., and W. Spakman, Structure and dynamics of subducted lithosphere in the Mediterranean region, *Proc. K. Ned. Akad. Wet.*, *95*, 325–347, 1992.

Wortel, M. J. R., and W. Spakman, Subduction and slab detachment in the Mediterranean-Carpathian region, *Science*, *290*, 1910–1917, 2000.

Zhou, H., and H. Wang, A revisit to P wave travel time statics at teleseismic stations, *J. Geophys. Res.*, *99*, 17,849–17,862, 1994.

Ziegler, P. A., European Cenozoic rift system, *Tectonophysics*, *208*, 91–111, 1992.

Zielhuis, A., and G. Nolet, Shear-wave velocity variations in the upper mantle beneath central Europe, *Geophys. J. Int.*, *117*, 695–715, 1994.

A. Morelli and C. Piromallo, Istituto Nazionale di Geofisica e Vulcanologia, Via di Vigna Murata 605, I-00143, Rome, Italy. (piromallo@ingv.it)